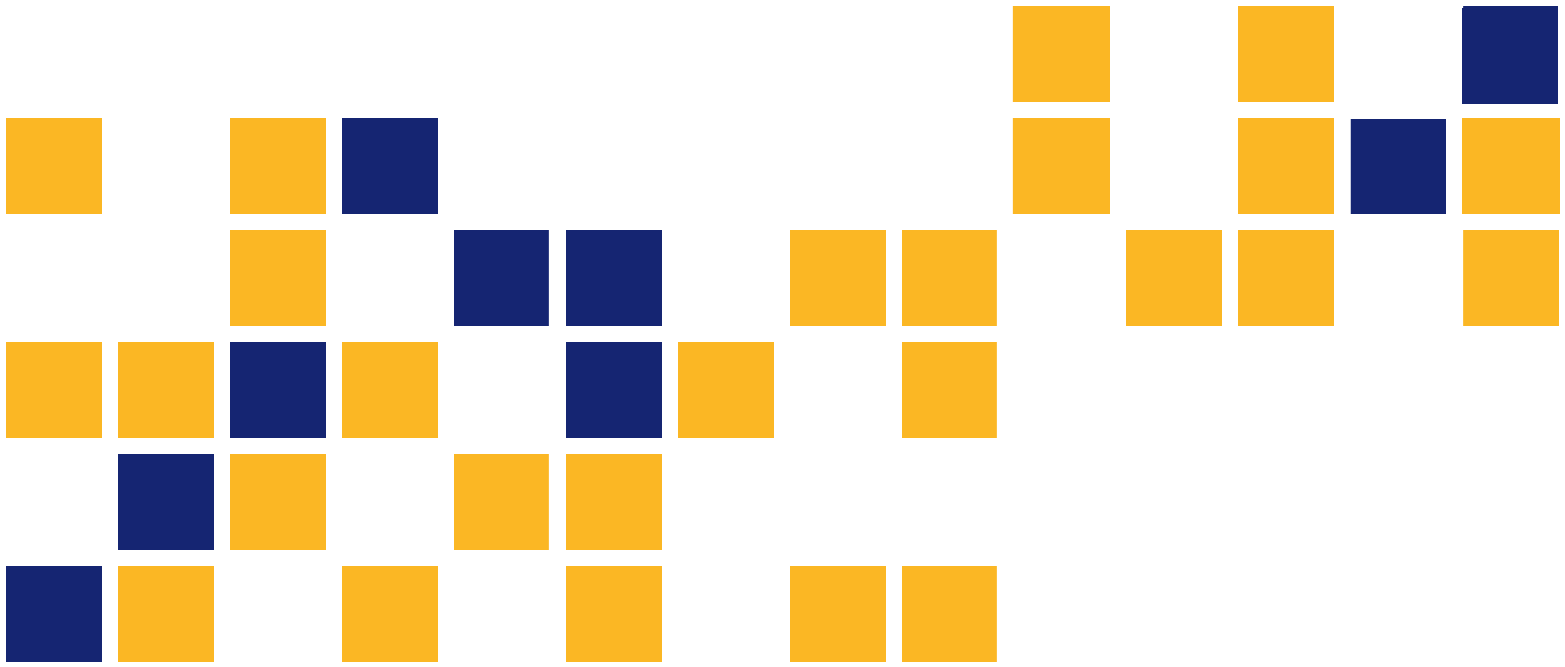


Evaluation and Long-Term Monitoring of the Time-Dependent Characteristics of Self-Consolidating Concrete in an Instrumented Kansas Prestressed Concrete Bridge

Joey Holste
Robert J. Peterman, Ph.D., P.E.
Asad Esmaily, Ph.D., P.E.
Kansas State University Transportation Center



A cooperative transportation research program between
Kansas Department of Transportation,
Kansas State University Transportation Center, and
The University of Kansas

This page intentionally left blank.

1 Report No. K-TRAN: KSU-10-8	2 Government Accession No.	3 Recipient Catalog No.	
4 Title and Subtitle Evaluation and Long-Term Monitoring of the Time-Dependent Characteristics of Self-Consolidating Concrete in an Instrumented Kansas Prestressed Concrete Bridge		5 Report Date January 2014	
		6 Performing Organization Code	
7 Author(s) Joey Holste; Robert J. Peterman, Ph.D., P.E.; Asad Esmaily, Ph.D., P.E.		8 Performing Organization Report No.	
9 Performing Organization Name and Address Department of Civil Engineering Kansas State University Transportation Center 2118 Fiedler Hall Manhattan, Kansas 66506		10 Work Unit No. (TRAIS)	
		11 Contract or Grant No. C1842	
12 Sponsoring Agency Name and Address Kansas Department of Transportation Bureau of Research 2300 SW Van Buren Topeka, Kansas 66611-1195		13 Type of Report and Period Covered Final Report October 2009–August 2013	
		14 Sponsoring Agency Code RE-0527-01	
15 Supplementary Notes For more information, write to address in block 9.			
16 Abstract <p>Construction of a new prestressed bridge with Self-Consolidating Concrete (SCC) provided the opportunity to further study the time-dependent properties of SCC mix and its long-term performance; considering the results and recommendations of previous studies on SCC conducted by the authors.</p> <p>This report discusses the instrumentation of three girders installed on the new Amelia Earhart Bridge (the Atchison River Bridge Project, 59-3 K-8238-02) to evaluate the long term performance of a SCC mix used in the prestressed concrete bridge girders. It describes the fabrication of the three girders and the measures taken for instrumentation at this stage, transportation of the girders to the erection site, instrumentation of the girders to be monitored on the site, the procedure for data collection, and long-term monitoring of the three instrumented girders.</p> <p>Vibrating wire strain gages were the main strain measurement instrument installed at pre-determined spots in the girders to determine long term losses. The girders were monitored for over three years. Creep and shrinkage prisms were also cast and measured to accurately determine creep and shrinkage variables for the concrete mix used. Strain measurements were used to evaluate the long-term losses.</p> <p>These values were then compared to ACI, PCI, and AASHTO code equations for girders under the same conditions. The measured losses were found to be less than the losses predicted by the aforesaid code equations. Comparison of the experimental values with the values calculated by the existing code procedures, shows that the actual values of losses are less than the values predicted by the procedures suggested by codes within the monitoring period in this study.</p>			
17 Key Words Prestressed Concrete, Bridge, Creep, Strain, Shrinkage, Structures		18 Distribution Statement No restrictions. This document is available to the public through the National Technical Information Service www.ntis.gov .	
19 Security Classification (of this report) Unclassified	20 Security Classification (of this page) Unclassified	21 No. of pages 100	22 Price

Form DOT F 1700.7 (8-72)

**Evaluation and Long-Term Monitoring of the Time-Dependent
Characteristics of Self-Consolidating Concrete in an Instrumented Kansas
Prestressed Concrete Bridge**

Final Report

Prepared by

Joey Holste
Robert J. Peterman, Ph.D., P.E.
Asad Esmaeily, Ph.D., P.E.

Kansas State University Transportation Center

A Report on Research Sponsored by

THE KANSAS DEPARTMENT OF TRANSPORTATION
TOPEKA, KANSAS

and

KANSAS STATE UNIVERSITY TRANSPORTATION CENTER
MANHATTAN, KANSAS

January 2014

© Copyright 2014, **Kansas Department of Transportation**

PREFACE

The Kansas Department of Transportation's (KDOT) Kansas Transportation Research and New-Developments (K-TRAN) Research Program funded this research project. It is an ongoing, cooperative and comprehensive research program addressing transportation needs of the state of Kansas utilizing academic and research resources from KDOT, Kansas State University and the University of Kansas. Transportation professionals in KDOT and the universities jointly develop the projects included in the research program.

NOTICE

The authors and the state of Kansas do not endorse products or manufacturers. Trade and manufacturers names appear herein solely because they are considered essential to the object of this report.

This information is available in alternative accessible formats. To obtain an alternative format, contact the Office of Transportation Information, Kansas Department of Transportation, 700 SW Harrison, Topeka, Kansas 66603-3754 or phone (785) 296-3585 (Voice) (TDD).

DISCLAIMER

The contents of this report reflect the views of the authors who are responsible for the facts and accuracy of the data presented herein. The contents do not necessarily reflect the views or the policies of the state of Kansas. This report does not constitute a standard, specification or regulation.

Abstract

Construction of a new prestressed bridge with Self-Consolidating Concrete (SCC) provided the opportunity to further study the time-dependent properties of SCC mix and its long-term performance; considering the results and recommendations of previous studies on SCC conducted by the authors.

This report discusses the instrumentation of three girders installed on the new Amelia Earhart Bridge (the Atchison River Bridge Project, 59-3 K-8238-02) to evaluate the long term performance of a SCC mix used in the pre-stressed concrete bridge girders. It describes the fabrication of the three girders and the measures taken for instrumentation at this stage, transportation of the girders to the erection site, instrumentation of the girders to be monitored on the site, the procedure for data collection, and long-term monitoring of the three instrumented girders.

Vibrating wire strain gages were the main strain measurement instrument installed at pre-determined spots in the girders to determine long term losses. The girders were monitored for over three years. Creep and shrinkage prisms were also cast and measured to accurately determine creep and shrinkage variables for the concrete mix used. Strain measurements were used to evaluate the long-term losses.

These values were then compared to ACI, PCI, and AASHTO code equations for girders under the same conditions. The measured losses were found to be less than the losses predicted by the aforesaid code equations. Comparison of the experimental values with the values calculated by the existing code procedures, shows that the actual values of losses are less than the values predicted by the procedures suggested by codes within the monitoring period in this study.

Table of Contents

Abstract	v
Table of Contents	vi
List of Tables	viii
List of Figures	ix
Chapter 1: Introduction	1
1.1 Objective	3
1.2 Location and Layout	3
1.3 Scope	5
Chapter 2: Literature Review	6
Chapter 3: Girder Fabrication and Installation	13
3.1 Fabrication	13
3.2 Transportation	17
3.3 Erection	18
3.4 Deck Pour	19
3.5 Bridge Completion	23
Chapter 4: Monitoring System	25
4.1 Details	25
4.2 Installation	27
4.3 Monitoring	37
4.4 Final Installation and Hookup	39
4.5 Deck Installation	41
Chapter 5: Monitoring Results	44
5.1 Strain along Beam Height	44
5.2 Prestress Losses	47
5.3 Comparison to Code	49
Chapter 6: Creep and Shrinkage Prisms	50
6.1 Creep	50
6.2 Shrinkage	52
6.3 Creep Results	52
6.4 Shrinkage Results	56

6.5 ACI 209 Prestress Loss Summary	60
Chapter 7: Conclusions and Recommendations	61
References	63
Appendix A: Girder Mix Properties	65
Appendix B: Girder Calculations.....	68
B.1 Prestress Loss Equations	68
B.2 Prestress Loss Calculations for Spans 1 and 2	70
B.3 Prestress Loss Calculations for Span 3	73
B.4 ACI 209 Prestress Loss Equations and Calculations	75
Appendix C: Additional Graphs	81

List of Tables

TABLE 5.1 Summary of Calculated Losses	49
TABLE 6.1 Summary of Creep and Shrinkage Parameters.....	56
TABLE 6.2 Summary of ACI 209 Losses	60

List of Figures

FIGURE 1.1 Old and New Amelia Earhart Bridges.....	3
FIGURE 1.2 Map of Kansas Showing Atchison	4
FIGURE 1.3 Overhead View of Bridges	4
FIGURE 1.4 Monitored Girder Location.....	5
FIGURE 1.5 Gage Locations along the Three Spans Being Monitored.....	5
FIGURE 3.1 Girder Reinforcement	13
FIGURE 3.2 Formwork For the Girders	14
FIGURE 3.3 Concrete Truck Dumping into Hopper	15
FIGURE 3.4 Hopper Being Dumped into Forms	15
FIGURE 3.5 Strand Being Cut with Torch.....	16
FIGURE 3.6 Girder Being Loaded onto Truck Using Two Cranes.....	17
FIGURE 3.7 Girder Secured to Trailer	18
FIGURE 3.8 Girder Secured to Trailer	18
FIGURE 3.9 Deck Reinforcement in Place	19
FIGURE 3.10 Deck Being Poured	20
FIGURE 3.11 Deck Being Poured	20
FIGURE 3.12 Deck Being Poured	21
FIGURE 3.13 Deck Being Finished	21
FIGURE 3.14 Deck Finished	22
FIGURE 3.15 Deck Covered in Burlap	22
FIGURE 3.16 Traffic Being Diverted onto New Bridge as the Old Bridge Is Being Removed ..	23
FIGURE 3.17 Old Bridge Abutment Being Removed to Make Room for New Bridge	24
FIGURE 4.1 Geokon Model 4202 Vibrating Wire Strain Gage.....	25
FIGURE 4.2 Geokon Model 8032 Multiplexer	26

FIGURE 4.3 Geokon Model 8021 Data Logger	27
FIGURE 4.4 VWSG Secured in Beam Reinforcement	28
FIGURE 4.5 VWSG Secured in Beam Reinforcement	28
FIGURE 4.6 VWSG Secured in Beam Reinforcement	29
FIGURE 4.7 VWSGs at End Part of Beam	29
FIGURE 4.8 Two VWSGs Secured near Bottom of Beam at Center Span.....	30
FIGURE 4.9 VWSG Locations at Center Span of Beam	30
FIGURE 4.10 PVC Elbow with Wires through It Secured on Flange of Beam before Casting...	31
FIGURE 4.11 Conduit Secured to Beam	32
FIGURE 4.12 Wires Run through Conduit.....	33
FIGURE 4.13 Wires Run through Conduit.....	33
FIGURE 4.14 Finished Conduit.....	34
FIGURE 4.15 Sealed Junction Boxes	34
FIGURE 4.16 Sealed Conduit System	35
FIGURE 4.17 Flexible Conduit with Cable.....	36
FIGURE 4.18 End Connection of Girder.....	36
FIGURE 4.19 Gage Readings Being Manually Taken	37
FIGURE 4.20 Temporary Wiring of the Data Logger in the Storage Yard.....	38
FIGURE 4.21 PVC Tube Run through the Diaphragm	39
FIGURE 4.22 PVC Tube Run through the Diaphragm	40
FIGURE 4.23 Cable Being Connected	40
FIGURE 4.24 Cable Connected and Secured	41
FIGURE 4.25 Deck Gage Mounted in Deck Reinforcement.....	42
FIGURE 4.26 Wiring from PVC Elbow that Was Cast in the Girder	42
FIGURE 4.27 Wiring from Gage to PVC Elbow	43

FIGURE 5.1 Strain Overtime for Each Gage on West End of Span 1	44
FIGURE 5.2 Strain Overtime for Each Gage in Center of Span 1	45
FIGURE 5.3 Strain Overtime for Each Gage on East End of Span 1	45
FIGURE 5.4 Strain along Height of West End of Span 1	46
FIGURE 5.5 Strain along Height of Middle of Span 1	46
FIGURE 5.6 Strain along Height of East End of Span 1	47
FIGURE 5.7 Effective Prestress in Span 1	48
FIGURE 5.8 Effective Prestress in Span 2	48
FIGURE 5.9 Effective Prestress in Span 3	49
FIGURE 6.1 Creep Specimens in Testing Frames	51
FIGURE 6.2 Creep Coefficient of T-Day #1	53
FIGURE 6.3 Creep Coefficient of T-Day #2	54
FIGURE 6.4 Creep Coefficient of T-Day #3	54
FIGURE 6.5 Creep Coefficient of 28-Day #1	55
FIGURE 6.6 Creep Coefficient of 28-Day #2	55
FIGURE 6.7 Creep Coefficient of 28-Day #3	56
FIGURE 6.8 Shrinkage Strains from T-Day #1	57
FIGURE 6.9 Shrinkage Strains from T-Day #2	58
FIGURE 6.10 Shrinkage Strains from T-Day #3	58
FIGURE 6.11 Shrinkage Strains from 28-Day #1	59
FIGURE 6.12 Shrinkage Strains from 28-Day #2	59
FIGURE 6.13 Shrinkage Strains from 28-Day #3	60
FIGURE A.1 Span 1 Mix Properties (Courtesy Ready Mixed Concrete)	65
FIGURE A.2 Span 2 Mix Properties (Courtesy Ready Mixed Concrete)	66
FIGURE A.3 Span 3 Mix Properties (Courtesy Ready Mixed Concrete)	67

FIGURE C.1 Strain Overtime for Each Gage on West End of Span 2.....	81
FIGURE C.2 Strain Overtime for Each Gage in Center of Span 2.....	81
FIGURE C.3 Strain Overtime for Each Gage on East End of Span 2	82
FIGURE C.4 Strain Overtime for Each Gage on West End of Span 3.....	82
FIGURE C.5 Strain Overtime for Each Gage in Center of Span 3.....	83
FIGURE C.6 Strain Overtime for Each Gage on East End of Span 3	83
FIGURE C.7 Strain along Height of West End of Span 2.....	84
FIGURE C.8 Strain along Height of Center of Span 2.....	84
FIGURE C.9 Strain along Height of East End of Span 2	85
FIGURE C.10 Strain along Height of West End of Span 3	85
FIGURE C.11 Strain along Height of Center of Span 3.....	86
FIGURE C.12 Strain along Height of East End of Span 3	86

Chapter 1: Introduction

Current use of prestressed concrete members is often accompanied by frequent “bug holes” in the bottom flange where direct vibration is not possible. Therefore, utilizing self-consolidating concrete (SCC) for the prestressed concrete members is a suitable option, which improves structural performance by proper consolidation, provides a smooth finish on the bottom flange and enhances durability and aesthetics.

Before SCC concrete can be implemented in these bridges, however, several critical material properties such as modulus of elasticity, shrinkage, creep, and bond characteristics of SCC concrete mixes must be quantified. Lower percentages of coarse aggregate and higher paste volumes are typical for SCC mixes compared to standard concrete with equal strength. Thus, SCC mixes exhibit lower elastic moduli, and higher shrinkage and creep characteristics.

Some preliminary investigations with SCC mixes had shown that the elastic modulus may be 20% lower than standard concrete mixes of equal strength, while the ultimate creep and shrinkage of these mixes can be 10% higher depending on mix design, as is typical for any type of concrete.

Considering the need to address these critical parameters and understand the performance of SCC, USDOT funded a research project to conduct a comprehensive study to evaluate the time-dependent and bond characteristics of a self-consolidating concrete mix for Kansas prestressed concrete bridges ("Evaluating the time-dependent and bond characteristics of a self-consolidating concrete mix for Kansas prestressed concrete bridges", R. J. Peterman, and A. Esmaily, 2003-2006).

In this study, a three-phase comprehensive experimental and analytical research program was conducted to evaluate a proposed self-consolidating concrete (SCC) mixture in prestressed bridge applications.

Phase I consisted of analyzing transfer lengths and development lengths of flexural specimens, phase II evaluated the transfer length of an inverted T-beam (IT) specimen by use of concrete surface strains along with monitoring long-term, time-dependent deformations, and phase III was to monitor long-term prestress losses of bridge girders cast with both conventional concrete and self-consolidating concrete as placed in the field.

The test program was undertaken due to concerns for the low pullout values while performing large-block pullout tests (LBPTs) with prestressing strand in SCC. It must be noted that results obtained in this study were specific for the proposed SCC mixture, and other SCC mixtures may have a different performance compared to the one tested in this program.

Complete details of the aforesaid experimental program, its main conclusions on the time dependent properties and bonding of the SCC used in the program, along with a number of recommendations based on the experimental results, plant observations and evaluation of other SCC mixtures; can be found in the report by Larson (2007).

As with any experimental program with a limited number of tests, the study did not provide any universal conclusions or recommendations. However, the following were among the recommendations based on this extensive research program: Current KDOT design guidelines should be used when SCC is to be used in state girders without any change.

General code equations for predicting modulus of elasticity (E_c) for the SCC mixture should not be used. The current equation overestimates the modulus of elasticity for the SCC mixture used in the study. This, justifies using experimental results for modulus, until a more accurate model is developed for SCC mixtures.

The research program had also some recommendations for the sites producing SCC structural members, such as monitoring the consistency of the SCC mixtures, eliminating long delays between placement of the SCC into the same girder, special precautions in hot weather, and training of state inspectors.

The aforesaid study recommends evaluation of other SCC mixtures that are to be used in bridge girders. One of the basic recommendations is placement of vibrating wire strain gages (VWSG) into a potential bridge girder cast with SCC which can serve as a good indicator to determine long-term prestress losses.

Designs accounting for long-term losses should be based on experimental measurements for the actual SCC mixture, rather than code expressions if any major difference is detected between the girder cast with SCC and code expressions, the research report adds, and the casting of separate girders to isolate shrinkage alone is not needed to determine total losses.

Construction of a new prestressed bridge with SCC (the Atchison River Bridge Project, 59-3 K-8238-02), provided the opportunity to further study the time-dependent properties of SCC mix and its long-term performance; considering the results and recommendations of the above study.

1.1 Objective

This report is the summary of the findings of over three and a half years of monitoring prestressed bridge girders of the new Amelia Earhart Bridge fabricated using self-consolidating concrete and normal concrete. These prestressed girders were instrumented and this report discusses the details and results of the long-term monitoring of their performance. The bridge replaced an older steel truss style bridge and was composed of prestressed girders and a steel arch in the middle. Figure 1.1 shows the old and new bridges side-by-side with the new bridge on the right.



FIGURE 1.1
Old and New Amelia Earhart Bridges

1.2 Location and Layout

The Amelia Earhart Bridge is located in Atchison, Kansas, crosses the Missouri River. Figure 1.2 shows a map of Kansas with Atchison marked on the top right corner and Figure 1.3 shows an overhead view of the bridge (Google 2013).



FIGURE 1.2
Map of Kansas Showing Atchison



FIGURE 1.3
Overhead View of Bridges

The monitored girders were on the west side of the bridge. They were the second girder from the south side of Spans 1-3. Figures 1.4 and 1.5 show the girder location and the location of the gages at each span, respectively.

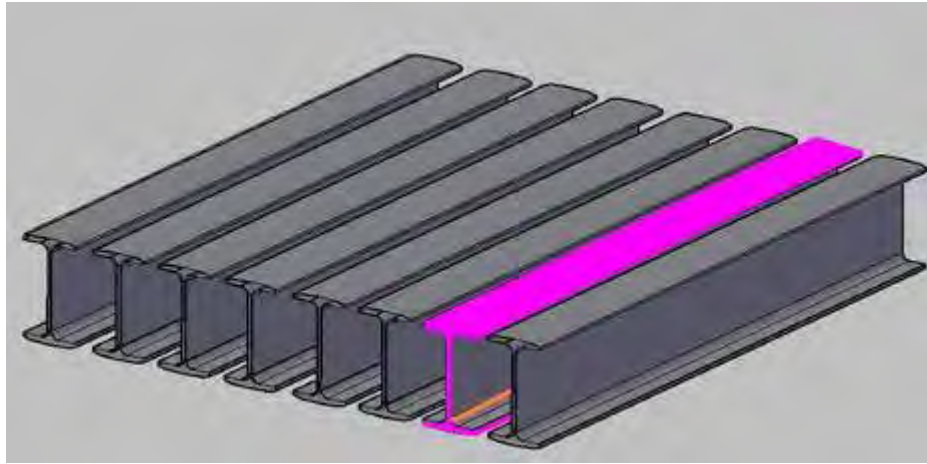


FIGURE 1.4
Monitored Girder Location

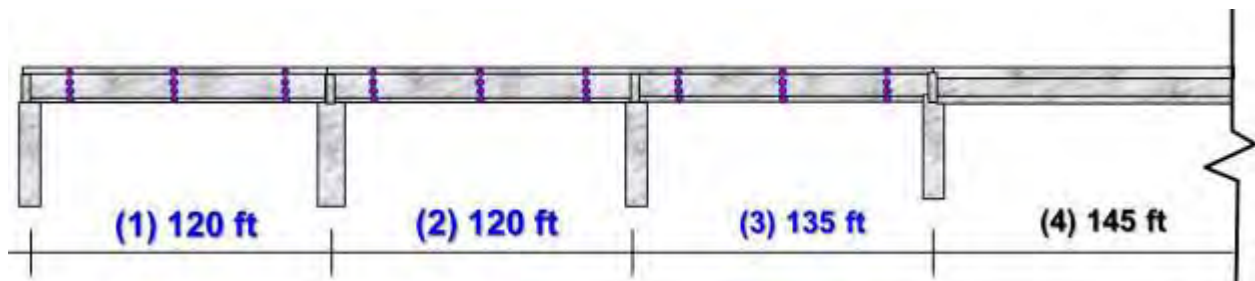


FIGURE 1.5
Gage Locations along the Three Spans Being Monitored

1.3 Scope

Chapter 2 reviews research that has been done on self-consolidating concrete, as well as various instrumentation methods used to monitor concrete members.

Chapter 3 describes fabrication of the girders that were monitored for this project.

Chapter 4 describes the installation of the monitoring system that was used in this study.

Chapter 5 reports the findings from the monitoring system and compares them to code equations.

Chapter 6 discusses the theory and fabrication of creep and shrinkage prisms used in this project and compares their findings to ACI 209 code equations.

Chapter 7 discusses conclusions and recommendations developed from this project.

Chapter 2: Literature Review

This section examines self-consolidating concrete and pre-stressing characteristics discussed in the author's master thesis (Holste 2010). It also reviews monitoring procedures done by Larson (2006).

Steinberg et al. (2001) monitored concrete strains that had developed from the cutting of the prestressing strand in pretensioned concrete beams. The study consisted of three rectangular prestressed concrete beams, 32 feet long and a cross section of 5 ½ x 23 inches. The reinforcement of the beams consisted of four ½-inch-diameter, seven-wire, grade 270, prestressed strand and #3 stirrups. Two of the prestressing strands were located 6 1/8 inches from the bottom of the beam and the other two were located two inches above that. The stirrups were spaced at 16-inch centers to provide the required shear capacity. The authors instrumented the beams with internal and external strain gages, external DEMEC points mounted to the beam, and linear variable differential transformers were mounted to the ends of the strands so that end-slip measurements could also be taken. The authors found that transfer lengths were all longer than the recommended amount of 25 inches. Internal strain gages were used to monitor the strain during release of the strands. Data acquisition used to monitor the internal strain gages used a sample rate of 7,500 readings per second to insure accurate readings from the gages. The authors found that longitudinal tensile strains had developed during the cutting of the prestressing strand. These strains were found to range from 50 to 150 microstrain, which could cause cracking in the member near its ends. The authors concluded that demountable mechanical strain (DEMEC) points and end-slip measurements were comparable methods of measuring the transfer length and that the strain gage results supported these two methods. The authors recommended future research should be done to verify the tensile strain results and to develop a more accurate transfer-length formula.

Weerasekera et al. (2008) summarized various methods used to measure bond and strains in concrete and steel due to prestressing. Various tests included beam tests, pullout tests, x-ray techniques, and the photo-elastic method. The authors developed an experiment to test the use of strain gages mounted to the prestressing strand versus use of DEMEC gage measurements to determine the strain in the concrete. The two methods varied largely throughout the transfer

length due to strand slip, but overall results for the entire beam were comparable for the two methods. The strain gage method required skilled techniques to attach the strain gages to the strand, and the gages were subject to damage during the testing process. The strain gages also change the surface condition of the strand by being glued to it. The DEMEC gage required a longer amount of time to take the required measurements and could become misleading at the point of a developing crack. The authors concluded that either techniques could be used to determine transfer length, and use of either technique would provide verification of the results from the testing.

Ouchi (2001) discussed the theory and use of self-compacting concrete in Japan. Self-compacting concrete (SCC) was developed to reduce the amount of skilled laborers needed to pour concrete for high-performance, durable structures. Ouchi explained how use of super-plasticizer could allow for a lower water-to-cement ratio and still allow the concrete mix to have a high workability. The super-plasticizer enables the mortar and the coarse aggregate to “flow” between the reinforcement bars but prevents segregation of the two. The SCC mixture requires little or no vibration due to its self-compaction through use of gravity. The author describes a project in Japan using SCC that decreased the number of skilled workers by 67% and completed the construction in 80% of the time required to finish the same project using non-SCC.

Khayat et al. (2004) analyzed various test methods available to test the performance of self-consolidating concrete (SCC). SCC has been increasing in popularity due to its flowable nature and reduced need for vibratory compaction. The authors tested various methods used to rate SCC mixes and compared the results. The test consisted of 16 SCC mixes whose water-to-cement ratios ranged from 0.32 to 0.47. The ratio of sand to coarse aggregate was kept the same for all mixes. High-range water-reducing admixture was used in all of the mixes and its amount was varied to produce the targeted slump. A set-retarding agent was used to maintain the targeted slump during testing. Each mix was tested with and without a viscosity-modifying admixture to test the changes in the mix. Each mixture was tested using the slump-cone, concrete rheometer, V-funnel, J-ring, L-box, U-box, and pressure-bleed tests, and all were given a visual stability index (VSI) rating. After comparing results from the tests, the authors had several conclusions. They found the slump and L-box or the slump and J-ring tests were both adequate to test the

passing nature and deformability of the SCC mixes. The authors also concluded the VSI rating could be used along with the other tests to greatly improve the evaluation of the SCC mixtures.

Girgis and Tuan (2005) researched bond characteristics of self-consolidating concrete. Testing included measuring transfer length of three girders, each poured using a specially designed mix. Two of the girders were cast using two specially designed SCC mixtures. The third girder, to be used as a control, was cast using a regular conventional mixture. The mixtures were tested for bond strength using a 0.6-inch-diameter strand with the Moustafa (1974) pullout test. Testing showed all three mixes had pullout strengths greater than the 36 kips recommended by Moustafa (1974). The girders were mounted with DEMEC points to measure transfer lengths of the three mixtures. The two SCC mixtures had transfer lengths, at 36 and 43 inches, that averaged longer than the American Concrete Institute (ACI) -recommended 30 inches. The control mix girder had an average transfer length of 20 inches. Compressive strength of the control mix was higher than the SCC mixes, which could account for shorter transfer lengths. The authors concluded that SCC mixes may have longer transfer lengths than conventional mixes and that future research is needed to verify these results.

Larson et al. (2007) tested bond properties of self-consolidating concrete. Transfer and development-length equations were tested by casting SCC beams that had been monitored for transfer and development length. Various cross sections were used to test the development length, and one cross section tested the effect of a top strand and its bonding characteristics. The strand used for these beams was tested using the pullout method recommended by Moustafa (1974) to verify the bonding quality of the SCC mixture. Pullout tests showed the recommended values by Moustafa (1974) should only be used for conventional mixes, and a higher value should be expected for SCC mixtures. Transfer-length results showed that equations proposed by American Association of State Highways and Transportation Officials (AASHTO) and ACI were acceptable for determining the transfer lengths of SCC mixtures. Transfer lengths were found to increase over the first 21 days after detensioning. This increase was more pronounced in the top strand, which increased on average, 40% to 45%. Bottom strand transfer lengths were found to increase 10% to 20%. Flexural testing on the SCC beams showed that equations for 100% and 80% embedment lengths were conservative in predicting the nominal moment capacity of the

SCC flexure beams. The 100% embedment lengths held 10% to 20% more than predicted, and the 80% beams held 25% to 35% more load than predicted. The authors concluded that the SCC mixture performed adequately well and the AASHTO and ACI equations, while conservative, can be used dependably to predict behavior of SCC mixes and beams.

Shing et al. (2000) reviewed the ACI and AASHTO transfer and development length equations for high-strength concrete box girders. The authors constructed three test specimens to verify the ACI and AASHTO formulas for transfer and development lengths when using high-strength concrete. The experiment consisted of three, 15-inch-wide and 21.75-inch-tall girders with a span of 33.4 feet. Nine-grade 270 low-relaxation 0.6-inch-diameter, seven-wire prestressing strands were used for flexural reinforcement, and #3 rebar stirrups were used as shear reinforcement. The girders were fabricated at Rocky Mountain Prestress in Boulder, Colorado, using a mix with a transfer strength of 6,500 psi and 56-day strength of 10,000 psi. The girders had embedded points at the level of the 0.6-inch-diameter strand and were measured with a Whittemore gauge before and after detensioning to accurately measure the transfer lengths. End-slip measurements were also used to verify the transfer lengths. The specimens were then tested to determine development lengths and were monitored for end-slip using linear voltage differential transducers (LVDT) attached to the strands at each end of the beam. The authors discovered the ACI and AASHTO formulas had overestimated the transfer and development lengths when using high-performance concrete. The transfer length equations were overestimated by 18% and the development lengths were overestimated by 53%. Bond characteristics of the prestress strand were also investigated in the project. The strand came from Insteel Wire Products and had a small amount of rust on it. It was tested for bond strength using the Moustafa pullout block method. Average strength of the pullout tests was 48.3 kips, which was greater than the 36 kips advised by Logan (1997) for 0.5-inch-diameter strand.

Buckner (1995) reviewed various equations that had been developed by other researchers in regard to transfer and development lengths for prestressed members. He explained that code equations needed to be changed due to the fact that most precasters use grade 270 instead of the earlier version grade 250 seven-wire strand. The older equations were developed based on the area of the grade 250 strand, with the grade 270 strand is six percent larger. Buckner

recommended increasing transfer lengths by 20% due to the higher jacking force the grade 270 strand experiences and the variation in the perimeters of the two grades of strand. Development length was also recommended to be increased by at least 1.7 times to allow for strength and ductility in the prestressed members.

Peterman (2007) tested the relationship of strand depth in relation to strand bond, and the effect of strand bond with relation to fluidity of the concrete. Three main tests were performed to determine these characteristics. The first consisted of casting beams at six different precast plants across the United States. Two different rectangular cross sections were cast, including 10 inches x 15 inches, 8 inches x 6 inches. The 8-inch x 6-inch beam had a strand at a depth of 4 ½ inches from the top of the beam. The 10 inch x 15 inch beams consisted of half with a strand two inches from the top of the beam and the other half with the strand 13 inches from the top of the beam. The strand used for all the beams was ½-inch in diameter, unweathered strand, from the same roll of strand. The strand was delivered to each plant prior to testing. Mixes from each plant varied, but the author recorded the rheological properties for each mix and found no correlation between them and the measured transfer lengths. Transfer lengths were measured on all of the beams using end-slip measurements after release by flame-cutting. The author discovered from the first test that transfer length decreased as distance from the top of the beam increased. The second test consisted of improved cross sections to reduce confinement of the strand. The cross sections were four-inch-wide rectangular beams, two with a height of 16 inches and two with a height of 28 inches. The strand location consisted of a bottom strand two inches from the bottom of the beam and a strand every six inches above that. This caused the 16-inch beam to have three strands and the 28-inch beam to have five strands, enabling a relationship between the strand location to the top and bottom of each beam. The author found the relationship between the transfer lengths and distance of the strand from the top surface had a coefficient of determination of 0.83. The author also found no relation between the column segregation test results and transfer length values. The third test consisted of casting four-inch panels and testing them while monitoring the end-slip measurement of the panels. The panels had a width of 24 inches and two 1/2-inch-diameter strands 2 ½ inches from the top and six inches in from each side of the beam. Lengths of the panels were varied to test embedment lengths of 30, 45, and 60 inches. The panels

were cast using conventional and SCC mixes. The compressive strengths at 28 days were 6,850 psi and 6,985 psi for the SCC and conventional mixes, respectively. They were loaded to failure using a point load, and the SCC panels averaged a 30% lower nominal moment capacity than the conventional mix. Transfer lengths were also measured using end-slip measurements, and the SCC panels averaged a 30% longer transfer length than the conventional panels. The author concluded that location of the strand with regard to the top of the beam was more influential than the amount of concrete below the strand. The author also concluded that as fluidity of the concrete increases, transfer length also increases.

Russell and Burns (1996) investigated the transfer lengths that are present in 0.5-and-0.6 inch-diameter prestressing strand. The authors tested the transfer lengths of specimens while changing several variables: strand size and number per specimen, shape of the specimen, amount of mild steel reinforcement causing confinement, spacing of the strand, and presence of debonding strand. The test was used to compare results with the equations given by ACI and AASHTO. Transfer lengths were measured using end-slip readings and DEMEC points. The authors used a smoothed-line technique to create the strain profile along the beam, using DEMEC measurements. The authors explained that transfer length was 95% of the average max strain value on the strain profile. The research showed the amount of confinement on the strands did not increase the transfer lengths. The 0.6-inch-diameter strand was found to produce reliable and repeatable transfer lengths; however, these lengths were on average 36% longer than the 0.5-inch-diameter strand. The authors concluded the code equations should be amended for 0.6-inch-diameter strand to enable it to be used with at least a spacing of two inches. The amended code equation could also be used for the 0.5-inch-diameter strand to be a more conservative estimate of the transfer length.

Barnes et al. (2003) tested factors that cause transfer length to vary, including concrete strength, strand surface condition, method of prestress release, and time at which the transfer length is recorded. The authors tested the transfer length of 36 AASHTO Type I girders during this investigation. Testing showed that rusted strand experienced a shorter transfer length than brighter strand. Transfer lengths were also found to increase over time, with the average increase being between 10% to 20%. This increase was found to happen within the first 28 days after

transfer of the prestress force. The authors concluded that sudden release of prestress force increased transfer lengths of rusted prestressing strand by as much as 50% but had little effect on concrete with strengths higher than 7,000 psi.

Larson (2006) used vibrating wire strain gages to measure long term losses in bridge girders. The gages were connected to a multiplexer that was connected to a data logger that recorded the readings from the gages over time. The data logger was powered by a 12 volt battery that was charged by a solar panel. Some of the girders that were monitored were cast using self-consolidating concrete. The vibrating wire strain gages were cast into the girders at a precast plant and were connected to the multiplexor in the field for long term readings. The use of vibrating wire strain gages proved to be a good method for recording long term strain readings.

Chapter 3: Girder Fabrication and Installation

This chapter explains the fabrication of the girders. It also discusses the material properties of the concrete that was used in casting the girders; and the steps involved in transporting the girders.

3.1 Fabrication

The girders were fabricated at Concrete Industries, Inc., Lincoln, Nebraska. They were NU2000 type girders with span lengths of 120 feet, 120 feet, and 135 feet. The girders that were being monitored were cast within two weeks of each other. The girder from Span 1 (120 ft) was cast on April, 9th, 2010, Span 2 (120 ft) was cast on April 7th, 2010, and Span 3 (135 ft) was cast on March 31st, 2010. Each girder was reinforced with 0.6 inch diameter 270 ksi low relaxation prestressing strand and grade 60 epoxy coated stirrups. Reinforcement and forms of the girders are show in Figures 3.1 and 3.2, respectively.



FIGURE 3.1
Girder Reinforcement



FIGURE 3.2
Formwork For the Girders

At each pour, various tests were performed to test the material properties of the concrete that was being used for the girders. Cylinders for compressive and tensile strength were made following ASTM C31 and C192 (2009). Air and unit weight was tested by following ASTM C173 and C138 (2009), respectively. The spread test was done following ASTM C1611 (2009). The VSI was seen to be zero with no bleeding seen during the spread test. The J-Ring test was done and showed no blockage by the aggregate by following ASTM C1621 (2009). Appendix A

shows the results from all of the tests for each of the girders. The girders were cast using concrete mix trucks that would deliver 10 cubic yards of concrete at a time. The trucks would unload 5 cubic yards of concrete into a hopper that was then hoisted up above the forms with a crane and then dumped through a latch in the bottom. Figures 3.3 and 3.4 show a truck dumping into hopper and the hopper dumping into forms, respectively.



FIGURE 3.3
Concrete Truck Dumping into Hopper



FIGURE 3.4
Hopper Being Dumped into Forms

After the girder had been cast and the top finished, the forms were then covered with a large tarp. Steam pipes that ran underneath the forms were used to heat up the concrete and to decrease the curing time. The compressive cylinders were tested according to ASTM C39 (2009) and once the concrete cylinders strength reached 6,000 psi, the forms were removed and the girder was de-tensioned. The strands at one end of the girder were cut with an oxygen-acetylene torch as the jack released the load at the other end. Figure 3.5 shows the worker cutting the strands. The release strengths for each girder can be seen in the Appendix A.



FIGURE 3.5
Strand Being Cut with Torch

On Span 1, 12 of the strands were left three feet longer than the girder after de-tensioning so that it could be used to tie in at the abutment and pier diaphragms during the erection process. After de-tensioning, the camber was checked against the design values and then the girder was moved to the storage part of the plant. Two ShuttleLift gantry cranes were used to move the girder from the casting bed to the storage yard. Since multiple girders were used in the bridge, a

girder was poured each day and they were all stored in the yard. The girders were left in the yard until they were transported to the bridge location.

3.2 Transportation

Once the bridge location was prepared and ready, the girders were moved from the precast plant in Lincoln, Nebraska, to Atchison, Kansas. Since the bridge erection was spaced out over a period of a few months, each set of girders were taken at a separate time. The girders were loaded onto special trailers and secured for transport. Great care was taken in transporting the girders since any eccentric loading or twisting could cause damage to the girders. Figures 3.6 to 3.8 show a girder being loaded and secured.



FIGURE 3.6
Girder Being Loaded onto Truck Using Two Cranes



FIGURE 3.7
Girder Secured to Trailer



FIGURE 3.8
Girder Secured to Trailer

3.3 Erection

The girders were placed in the final location during May and June of 2010. Each set of girders were placed using cranes. Only the south girders of Span 1 were placed since the existing bridge's abutment was in the same location as the new abutment. All of the girders for spans 2 and 3 were placed next.

3.4 Deck Pour

The formwork of the deck was installed and the deck over Spans 1-3 was cast on July 13th, 2010. The deck was only cast on the girders that were installed since the layout of the bridge abutment required the old bridge to be removed before the new bridge's abutment to be finished. Figures 3.9-3.15 show the deck being poured and finished.

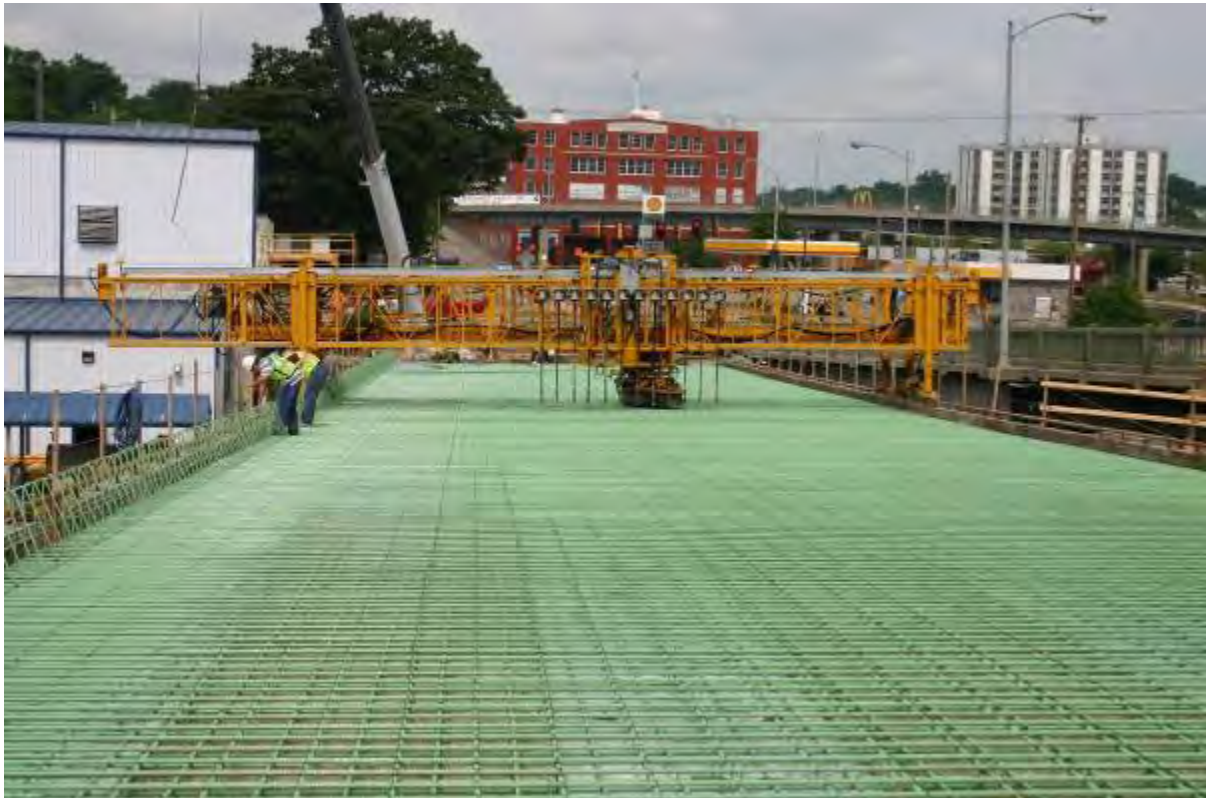


FIGURE 3.9
Deck Reinforcement in Place



FIGURE 3.10
Deck Being Poured



FIGURE 3.11
Deck Being Poured



FIGURE 3.12
Deck Being Poured



FIGURE 3.13
Deck Being Finished



FIGURE 3.14
Deck Finished



FIGURE 3.15
Deck Covered in Burlap

3.5 Bridge Completion

Traffic was diverted to the new bridge after the new bridge had been partially completed. After traffic was removed from the old bridge, the old abutment was torn down to make room for the new bridge's abutment. Figure 3.16 shows the traffic being diverted to the new bridge. Figure 3.17 shows the old abutment being tore down.



FIGURE 3.16
Traffic Being Diverted onto New Bridge as the Old Bridge Is Being Removed



FIGURE 3.17
Old Bridge Abutment Being Removed to Make Room for New Bridge

Chapter 4: Monitoring System

This chapter will explain the monitoring system that was used on the girders. It will also go through the installation and setup of the system. It also will discuss the steps involved in hooking up the system in the field and the process used to retrieve data.

4.1 Details

The monitoring system that was used consisted of three main components. These components were the gages, multiplexer, that the gages were wired to and the data logger that scanned and recorded the data. The gages that were used were vibrating wire strain gages from Geokon (Model 4202). The gage consisted of a wire connecting two end buttons and being protected by an outer tube. The wire was “plucked” magnetically in the middle and the resulting frequency was recorded. The gage also had a thermocouple in the middle section of the gage to record the temperature at each reading so that the change in temperature could be accounted for and not change the readings. Figure 4.1 shows one of the gages that was used.



FIGURE 4.1
Geokon Model 4202 Vibrating Wire Strain Gage

The multiplexer that was used was from Geokon (Model 8032). It was used to connect the gages from each girder together. After the gages were connected to the multiplexer, the multiplexer was connected to the data logger so that all of the gages could be scanned. Due to the setup of the girders, the multiplexer for Span 3 was daisy chained to Span 2's multiplexer and then connected to the data logger on Span 1. The multiplexer on Span 1 was connected directly to the data logger. Figure 4.2 shows the multiplexer that was installed on Span 1.



FIGURE 4.2
Geokon Model 8032 Multiplexer

The data logger that was used was from Geokon (Model 8021). It was used to scan each of the gages periodically and record the readings. The data logger was equipped with a modem and antenna that was used to download the data remotely. The data logger was also connected to a solar panel to be able to keep the battery charged. Figure 4.3 shows the data logger installed on Span 1.



FIGURE 4.3
Geokon Model 8021 Data Logger

4.2 Installation

The gages were embedded in the concrete girders. A total of 10 gages were installed in each girder. At each end of each girder, three gages were installed through the height of the girder. These gages were located four feet from the end of the girder and the approximate heights of the three gages were 4 inches, 36 inches, and 74 inches from the bottom of the girder. The locations of the gages were chosen so that the bottom gage was at the centroid of the pre-stress strand, the middle gage was at the centroid of the cross section, and the top gage was located to provide easy installation and was used to verify that the cross section remained plane after detensioning. The gages were attached to #3 bars using foam and plastic zip ties to provide vibration isolation from the rest of the reinforcement. The #3 bars were then connected to the girder shear reinforcement using wire ties. Figures 4.4 to 4.7 show the gages that were installed near the end of the beam.



FIGURE 4.4
VWSG Secured in Beam Reinforcement

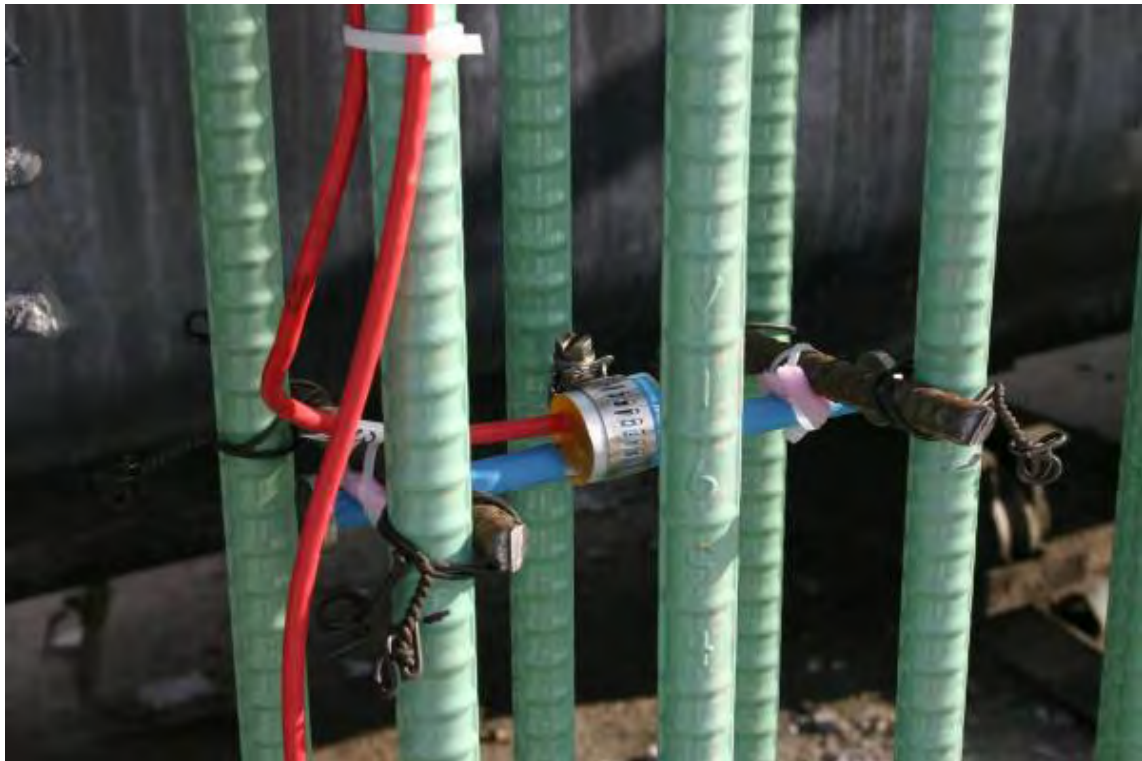


FIGURE 4.5
VWSG Secured in Beam Reinforcement



FIGURE 4.6
VWSG Secured in Beam Reinforcement



FIGURE 4.7
VWSGs at End Part of Beam

The remaining four gages were installed in the middle of the span. Two gages were used at the bottom location and one at the middle and one at the top. Two gages were used in the bottom since that measurement was critical for the calculations and using two gages would verify it and would also provide an extra reading if one of the gages would become inoperable. Figures 4.8 and 4.9 show the gages installed at the center of the span.



FIGURE 4.8
Two VWSGs Secured near Bottom of Beam at Center Span

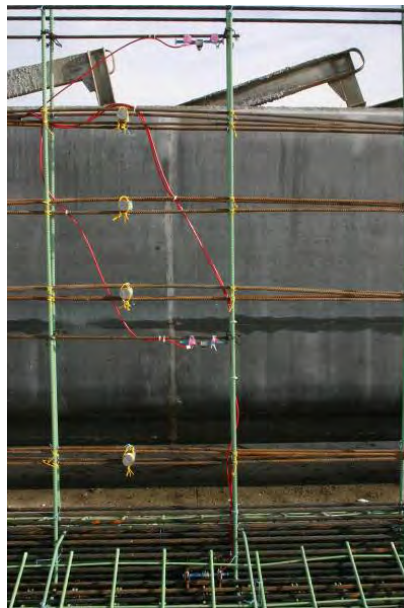


FIGURE 4.9
VWSG Locations at Center Span of Beam

The wires for the gages were looped through and ran to the top of the girder. There the extra length of wires was ran through a PVC elbow connection and then sealed in a plastic bag and taped to the top outside part of the forms where they would be protected during the pour. Figure 4.10 shows the gage wires ran outside of the PVC connection.



FIGURE 4.10
PVC Elbow with Wires through It Secured on Flange of Beam before Casting

After the each girder was cast, it was moved to the storage yard. Plastic conduit was installed along the bottom edge of the top flange. The conduit location was selected so that it was out of the way of the intermediate steel diaphragms that would be installed later. This conduit extended from the gage locations from each end of the girder. The conduit was used to protect the wires of each gage from getting cut or being exposed to the elements. The conduit was secured to the girder with concrete anchor screws and mounting brackets as seen in Figure 4.11.



FIGURE 4.11
Conduit Secured to Beam

The wires for each of the gages were routed through the PVC connection that was cast in the top flange through a hole in the flange. Next, the wires were run through conduit so that they all would go to the middle of the span. At the center span of the girder, the multiplexer was connected to the conduit so that the wires would be wired into the multiplexer and always be in conduit. Figures 4.12 to 4.16 show the wires run through the conduit and sealed system.



FIGURE 4.12
Wires Run through Conduit



FIGURE 4.13
Wires Run through Conduit



FIGURE 4.14
Finished Conduit

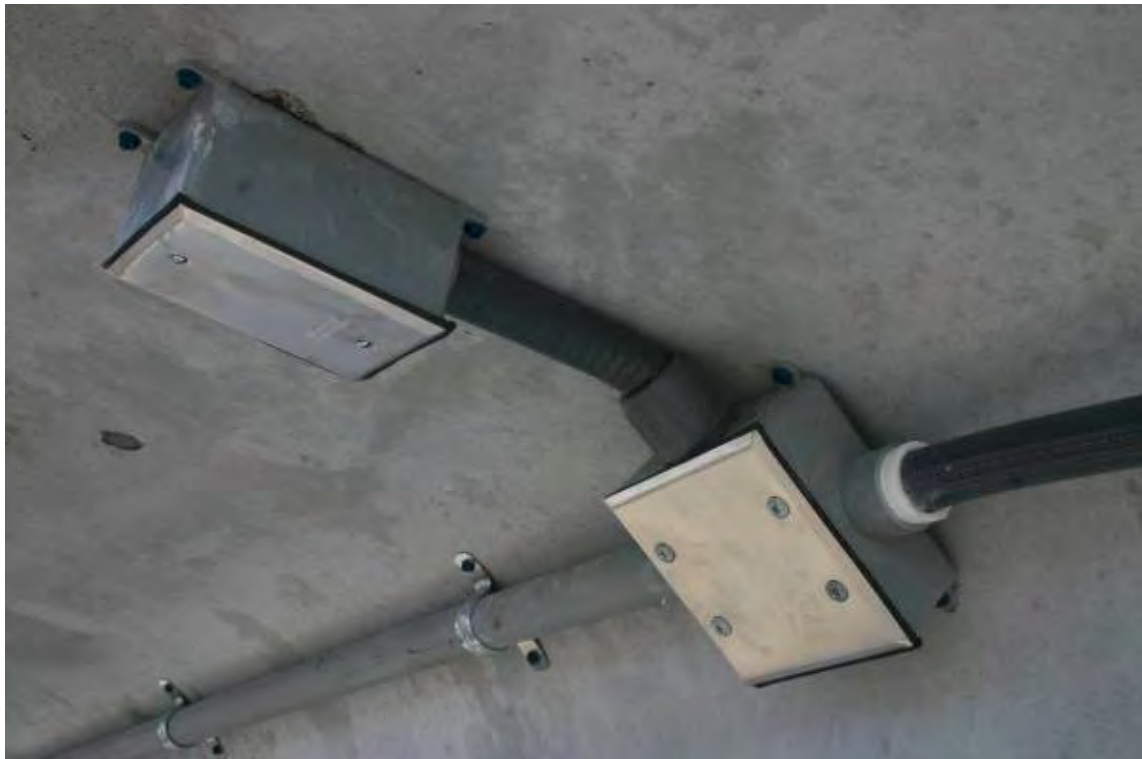


FIGURE 4.15
Sealed Junction Boxes



FIGURE 4.16
Sealed Conduit System

The cable that was used to connect the multiplexers to each other and the data logger was pulled through the same conduit. At the end of each girder, the cable used to connect the multiplexers and data logger was setup to be able to be connected when the girders were placed in the final location. It was put in a flexible conduit and secured to the girder until the girder was moved to its final location. The end of the cable had amphenol connectors installed to make the final connection process easier. A junction box was mounted on the girder to provide a safe place

to make the final connection. Figures 4.17 and 4.18 show the flexible conduit at the end of the girder.



FIGURE 4.17
Flexible Conduit with Cable



FIGURE 4.18
End Connection of Girder

4.3 Monitoring

Before detensioning, initial readings were taken of the VSWG's. These reading were the most important since all other readings were measured from these baseline readings. The gages were manually read using a Geokon GK 404 and two sets of readings were taken to verify accuracy. After detensioning, the gage readings were measured again since the automated monitoring system had not been installed yet. Figure 4.19 shows the readings being manually taken.



FIGURE 4.19
Gage Readings Being Manually Taken

After the girders were moved to the storage yard the readings were taken again manually one more time. The monitoring system was installed and the data logger started recording the readings. Temporary wiring between the girders was done while the girders were sitting in the storage yard since the girders were side by side and not end to end. The data logger was programmed to take readings every thirty minutes. These readings were stored in the data logger

until they were downloaded. The modem that was in the data logger enabled the data to be downloaded remotely however the large draw of power from the modem caused the data logger to stop recording after a few weeks so the modem was disconnected. Figure 4.20 shows the data logger setup with a modem antenna and temporary wiring.



FIGURE 4.20
Temporary Wiring of the Data Logger in the Storage Yard

After disconnecting the modem, a laptop was taken to the location and connected to the data logger whenever the data was to be downloaded and saved. The data that was collected was used to show the behavior of the girders over time. A few malfunctions in the battery supply caused there to be a few gaps in the data that was collected. The transportation and installation of the girders also caused a gap in the data that was collected but the amount that was collected was more than enough to make accurate calculations. The girders were monitored using the data logger throughout the time they were stored in the yard in Lincoln. When the girders were ready to move to Atchison, KS, the data logger was disconnected and removed for transport.

4.4 Final Installation and Hookup

After the girders were transported to Atchison, KS, they were set in place. The three spans needed to be connected together again so that the data logger could record readings. To connect the multiplexers from each girder together, the cable at the end of the girder needed to be ran through the diaphragm at each pier. A PVC tube was installed through the diaphragm at the pier. This tube was used as a conduit to pass the cable from one girder to the other. A man lift was used to access the two sides of the pier to pass the cable through. The cable was connected to the other cable on the next girder using amphenol connectors that had been installed at the plant. The cable was secured to the girder and the connection was sealed in a junction box. Figures 4.21 to 4.24 show the PVC run through the diaphragm and the connecting of the cable.



FIGURE 4.21
PVC Tube Run through the Diaphragm



FIGURE 4.22
PVC Tube Run through the Diaphragm

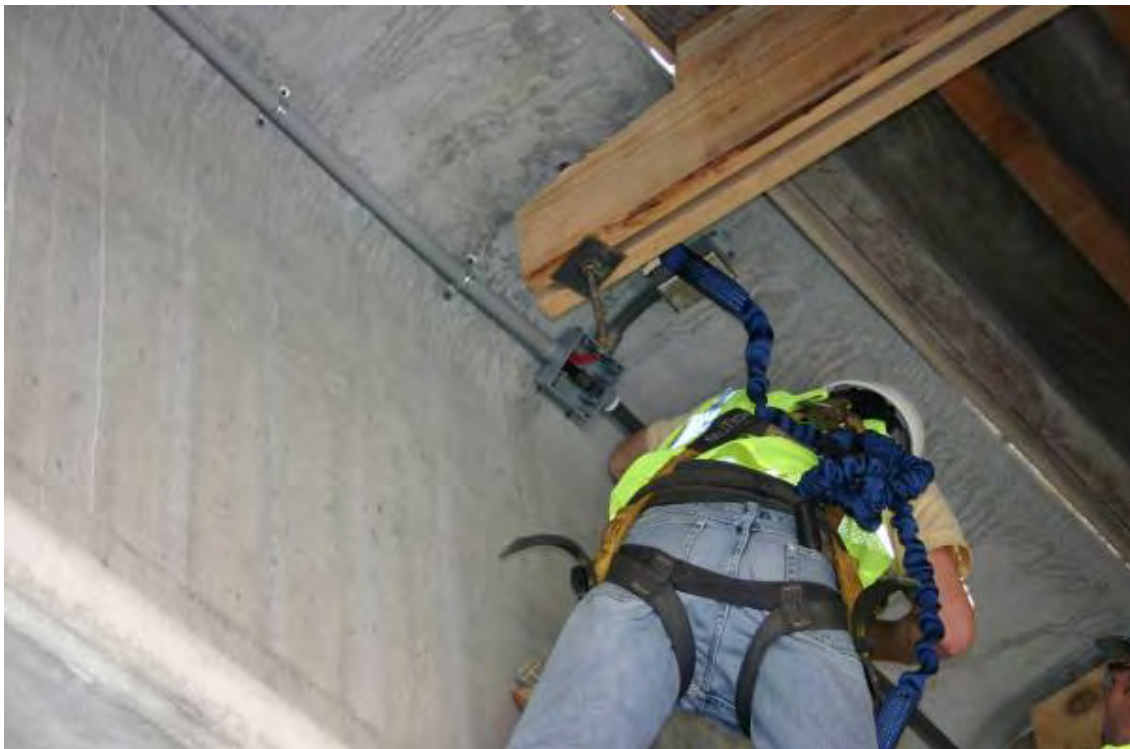


FIGURE 4.23
Cable Being Connected



FIGURE 4.24
Cable Connected and Secured

4.5 Deck Installation

After the girders had been placed, the formwork was installed for pouring the deck. The gages that were to be cast in the deck were attached to the deck reinforcement. The gages were secured to a special rebar template and mounted four inches from the top of the girder. The gages were connected to the cables that were stored in the connector that had been cast in the beam. These were the cables that were installed at the concrete plant. Figures 4.25 to 27 show the deck gage mounting and wiring setup.



FIGURE 4.25
Deck Gage Mounted in Deck Reinforcement



FIGURE 4.26
Wiring from PVC Elbow that Was Cast in the Girder



FIGURE 4.27
Wiring from Gage to PVC Elbow

Chapter 5: Monitoring Results

This section describes and discusses the findings from the vibrating wire strain gage data, and compares the monitoring results with code equations.

5.1 Strain along Beam Height

The data that was recorded with the data logger was used to plot the change in strain of the concrete at each gage location. The strain measurements were plotted overtime to see the long term behavior of the girders. Figures 5.1 to 5.3 show the readings over time for the three locations in Span 1. The west and east locations refer to the girder ends where the gage was installed. The measurements for Spans 2 and 3 can be seen in Appendix C.

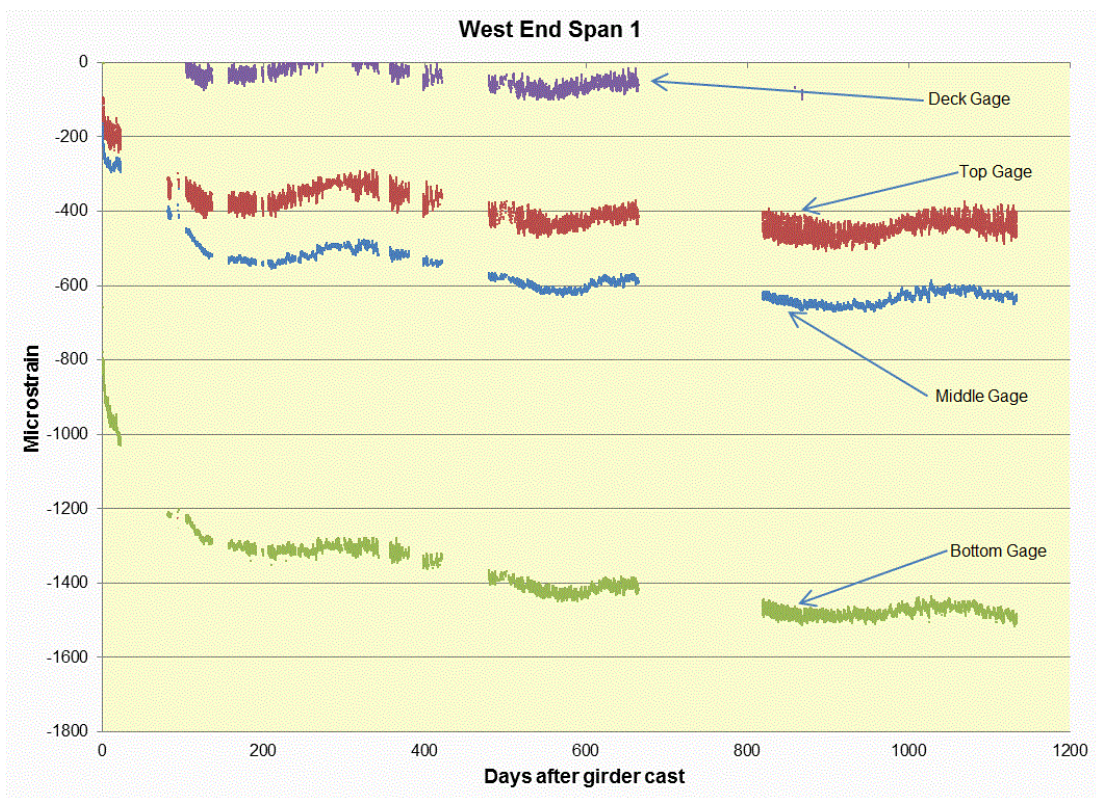


FIGURE 5.1
Strain Overtime for Each Gage on West End of Span 1

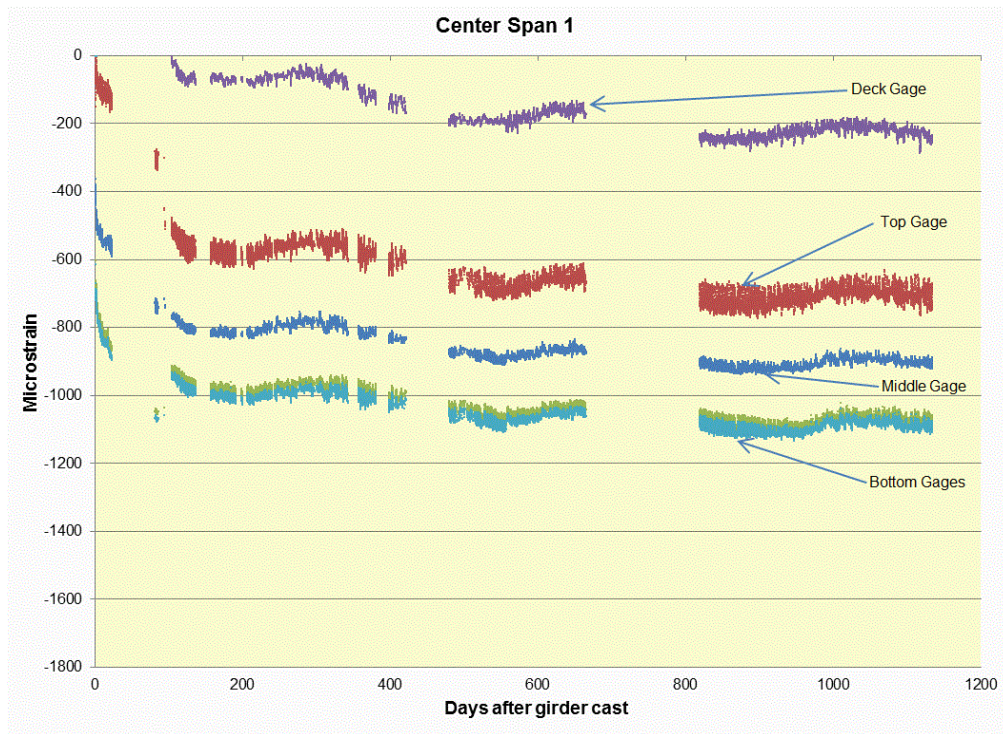


FIGURE 5.2
Strain Overtime for Each Gage in Center of Span 1

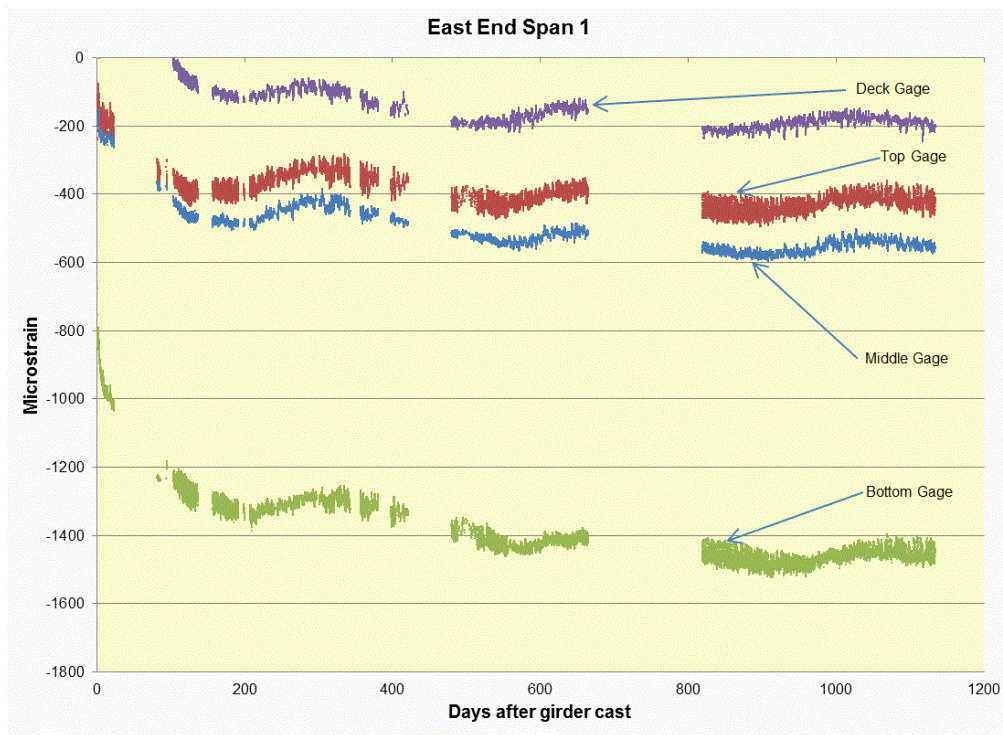


FIGURE 5.3
Strain Overtime for Each Gage on East End of Span 1

The strain along the height of the beam was plotted for selected time frames to see the behavior of the cross section due to the loading. The mid span of the girder remained plane along the cross section through the monitoring of the girder. The end locations did not remain plane due to the large amount of prestress force that was applied at the ends of the girder. The strain along the height of the beam in Span 1 can be seen in Figures 5.4 to 5.6. The graphs for Spans 2 and 3 can be seen in Appendix C.

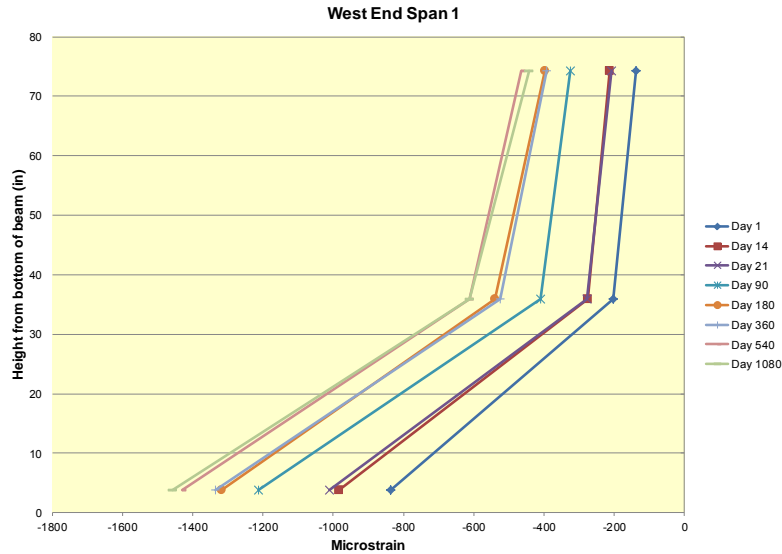


FIGURE 5.4
Strain along Height of West End of Span 1

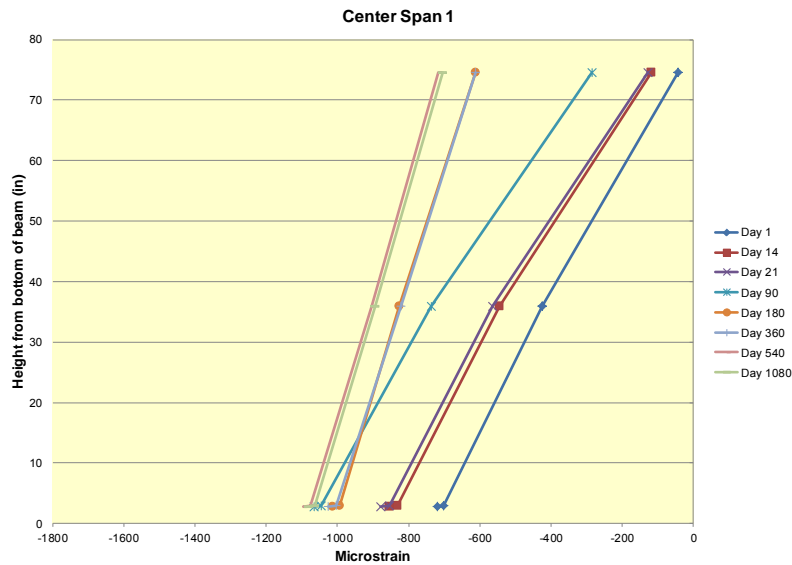


FIGURE 5.5
Strain along Height of Middle of Span 1

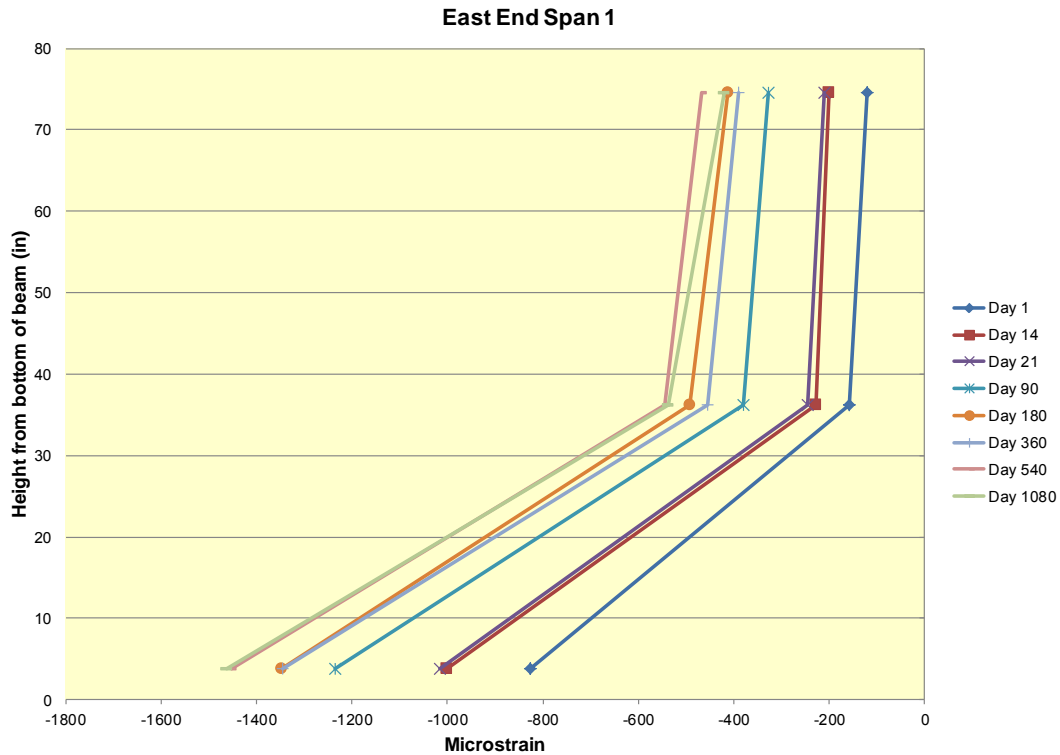


FIGURE 5.6
Strain along Height of East End of Span 1

5.2 Prestress Losses

The strain readings from the mid span bottom two gages were used to calculate the losses in the girder. Since the gages were mounted at the same location as the center of gravity of the prestressing strand, the change in strain found by the gages is equal to the change in strain of the strand. The readings from the two gages were averaged and multiplied by the modulus of the prestressing strand (28,500 ksi) to determine the amount of losses. The losses were subtracted from the initial stress in the strand (202.5 ksi) to determine the effective prestress. Figures 5.4 to 5.6 show the change in effective prestress with respect to time.

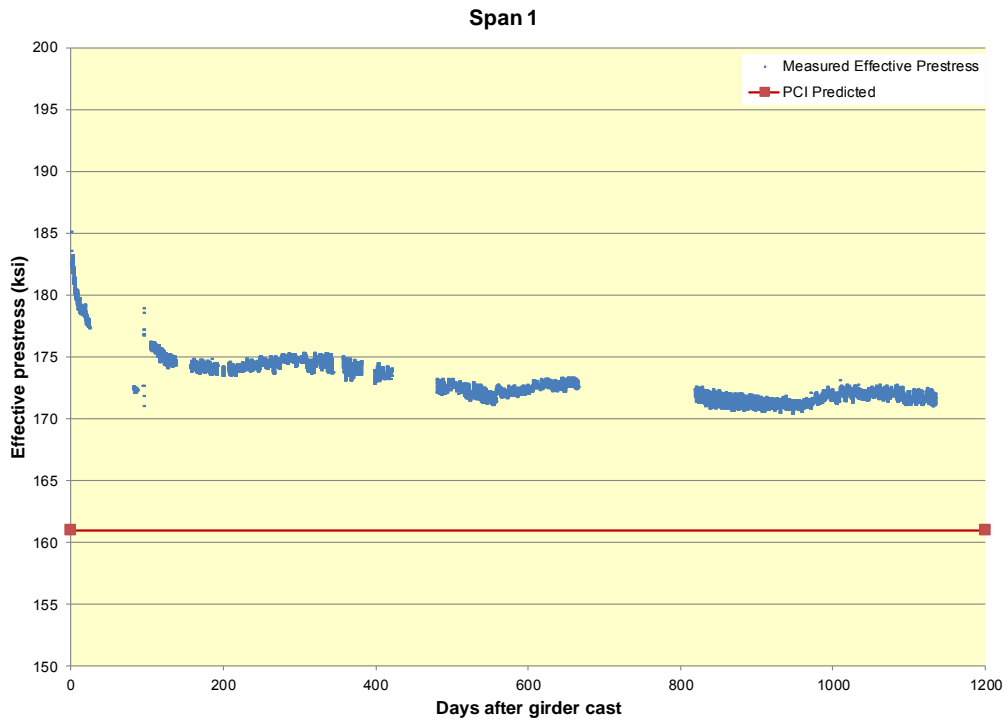


FIGURE 5.7
Effective Prestress in Span 1

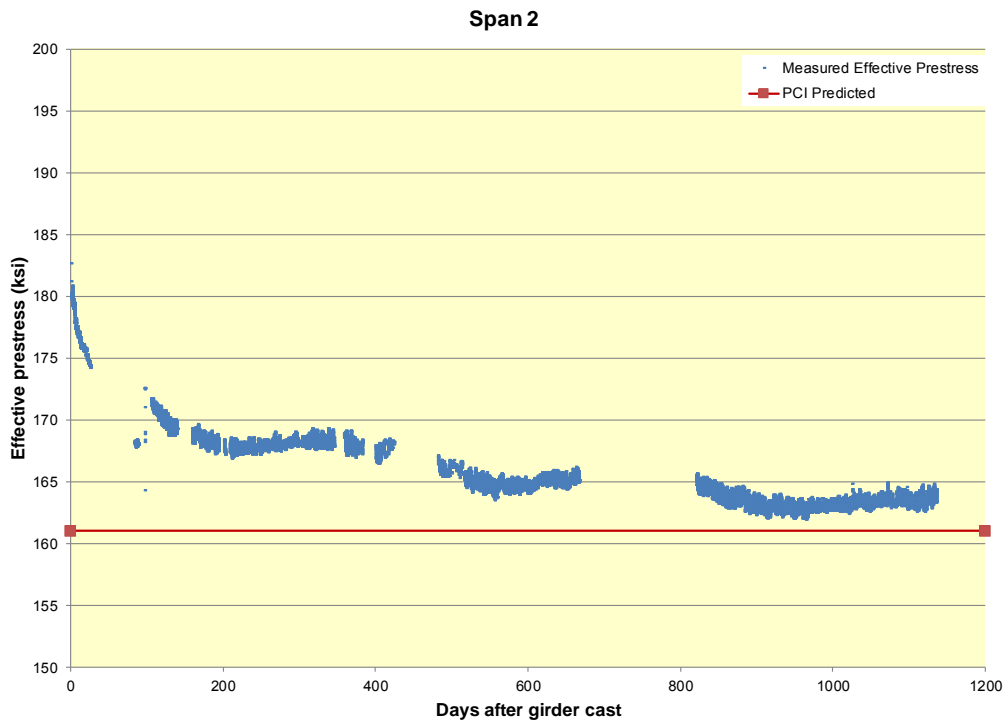


FIGURE 5.8
Effective Prestress in Span 2

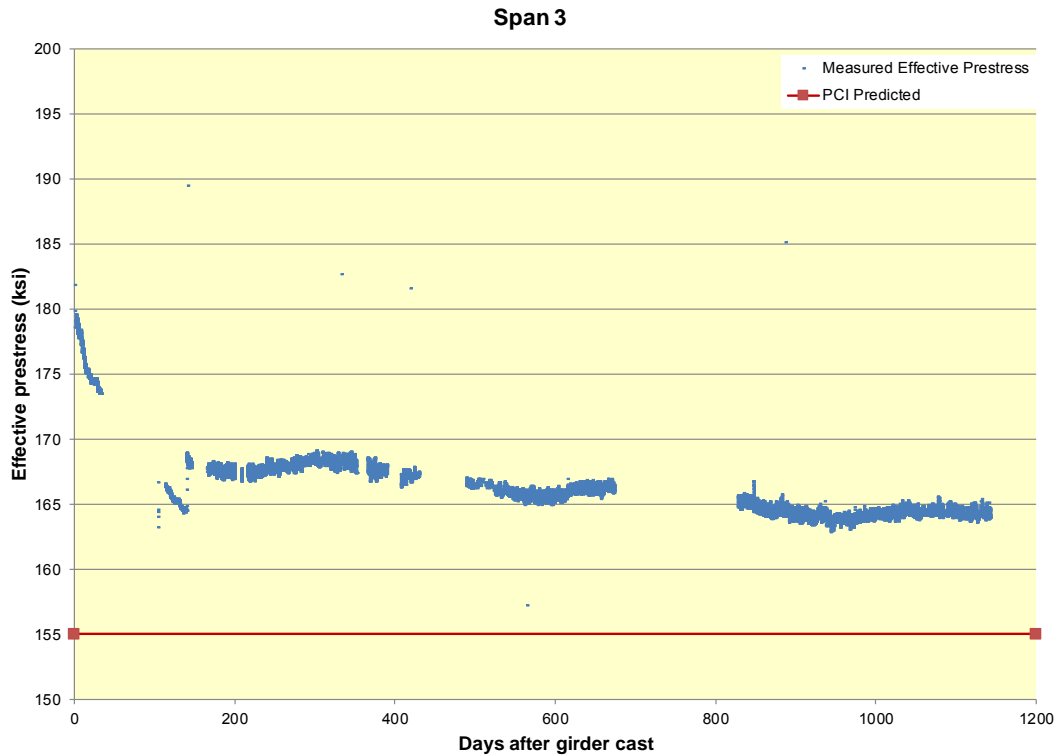


FIGURE 5.9
Effective Prestress in Span 3

5.3 Comparison to Code

The losses that were found in the girders were compared to the code equations. Code equations that were used to compare with the measured losses can be seen in Appendix B along with the calculations for each girder. Table 5.1 shows the summary of the calculated losses and compares them to the measured losses.

TABLE 5.1
Summary of Calculated Losses

	Elastic Shortening	Creep	Shrinkage	Relaxation	Effective Prestress
Spans 1 and 2	-	-	-	-	172/163
ACI/PCI	15.19	16.61	5.79	3.5	161
AASHTO	17.4	30.31	6.5	1.7	147
Span 3	-	-	-	-	164
ACI/PCI	18.14	19.93	5.79	3.25	155
AASHTO	20.8	36.34	6.5	0.9	138

*All values in ksi

Chapter 6: Creep and Shrinkage Prisms

This section discusses the theory equations, fabrication, and monitoring results of creep and shrinkage prisms that were cast for this study. These processes and methods were discussed earlier in the author's master thesis (Holste 2010).

6.1 Creep

Creep is defined as “the time-dependent increase of strain in hardened concrete subjected to sustained stress” (ACI Committee 209 2005). Prestressed beams experience a large amount of creep due to the prestressing force. It is important to know the amount of creep in a beam so that prestress losses due to creep can be estimated correctly. ACI Committee 209 (2005) has developed the following equation for predicting the amount of creep over time in a prestress beam:

$$v_t = \frac{t^\psi}{d + t^\psi} v_u \quad \text{Equation 6.1}$$

where:

- v_t = creep coefficient at time t
- d = constant (6 to 30 days)
- ψ = constant (0.40 to 0.80)
- t = time in days after loading
- v_u = ultimate creep coefficient (1.30 to 4.15)

The procedure from ATSM C512 (2009) was followed in testing the creep specimens. Six creep specimens were cast from the concrete mix used for the girders. These specimens were 4 inches by 4 inches square with a height of 24 inches. Three of the specimens were loaded at the time of detensioning the girders and the remaining three were loaded at 28 days. The specimens were mounted with Whittemore points to measure the strain. The top and bottom of each prism was sulfur-capped to provide an even surface to load the prisms on without causing any irregularities. The prisms were loaded to 40% of their compressive strength in load frames that can be seen in Figure 6.1.



FIGURE 6.1
Creep Specimens in Testing Frames

Whittemore readings were taken at the appropriate interval as prescribed by ASTM C512 (2009). Prisms were housed in an environmental chamber. Humidity was maintained at $50 \pm 4\%$ and temperature was maintained at 73.4 ± 2.0 degrees Fahrenheit as stated in ASTM C512 (2009).

6.2 Shrinkage

ACI Committee 209 (2005) states, “Shrinkage, after hardening of concrete, is the decrease with time of the concrete volume.” There are three types of shrinkage: “drying shrinkage due to moisture loss in the concrete, autogenous shrinkage caused by the hydration of cement, and carbonation shrinkage resulting as the various cement hydration products are carbonated in the presence of CO²”. ACI Committee 209 (2005) developed Equation 6.2 to predict the amount of shrinkage over time in a concrete beam. The amount of shrinkage can decrease the prestress force in a prestressed beam and is an important parameter to estimate.

$$(\epsilon_{sh})_t = \frac{t^\alpha}{f + t^\alpha} (\epsilon_{sh})_u \quad \text{Equation 6.2}$$

where:

$(\epsilon_{sh})_t$ = shrinkage strain at time t

t = time after loading

f = constant (20 to 130 days)

α = constant (0.90 to 1.10)

$(\epsilon_{sh})_u$ = ultimate shrinkage strain (415×10^{-6} to 1070×10^{-6})

Since each creep prism experienced shrinkage, a shrinkage prism was cast for each creep prism to be able to subtract the shrinkage from the creep values. The shrinkage prisms were mounted with Whittemore points and were measured at the same time as the creep prisms. The top and bottom of each prism was sulfur-capped to maintain the same volume-to-surface ratio as the creep prisms. The shrinkage prisms were housed in the same location as the creep prisms to prevent a variation in environmental changes.

6.3 Creep Results

Readings were taken from the creep specimens for almost one year. The creep readings included elastic shortening, creep strain, and shrinkage. The creep strains were calculated by subtracting the elastic shortening and shrinkage of the companion specimens from the total strain

readings. ACI Committee 209 (2005) stated that the creep coefficient can be found by graphing Equation 6.1 and changing the variables ψ , d , and V_u until the values fit the actual data. The experimental creep coefficient is the ratio found by dividing creep strains by the elastic shortening strain. The variables in Equation 6.1 can be varied until the data fits the graph of the experimental data. The creep coefficient variables were found using a trial-and-error method for both sets of specimens. Three of specimens were loaded at detensioning (T-Day), and three were loaded at 28 days (28-Day). Figures 6.2-6.4 show results from the first set of specimens loaded at detensioning. Figures 6.5-6.7 show results from the second set of specimens that were loaded at 28 days. Creep parameters for all of the specimens are summarized in Table 6.1.

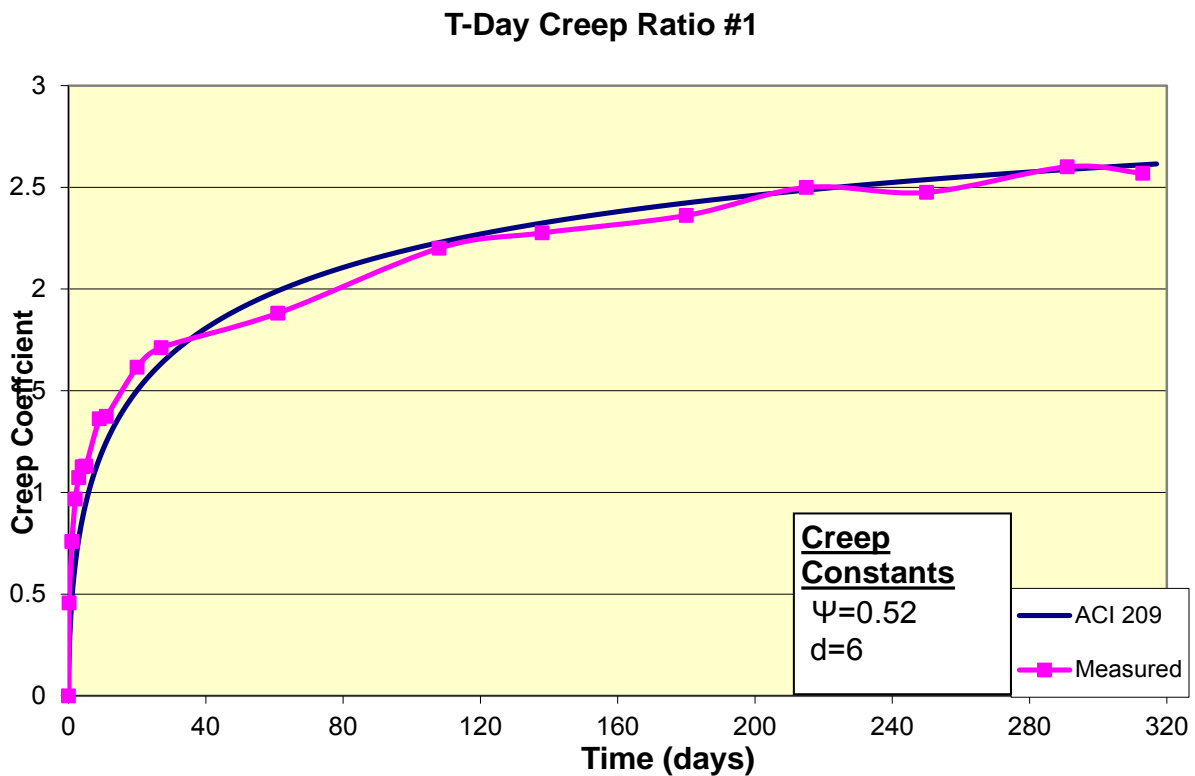


FIGURE 6.2
Creep Coefficient of T-Day #1

T-Day Creep Ratio #2

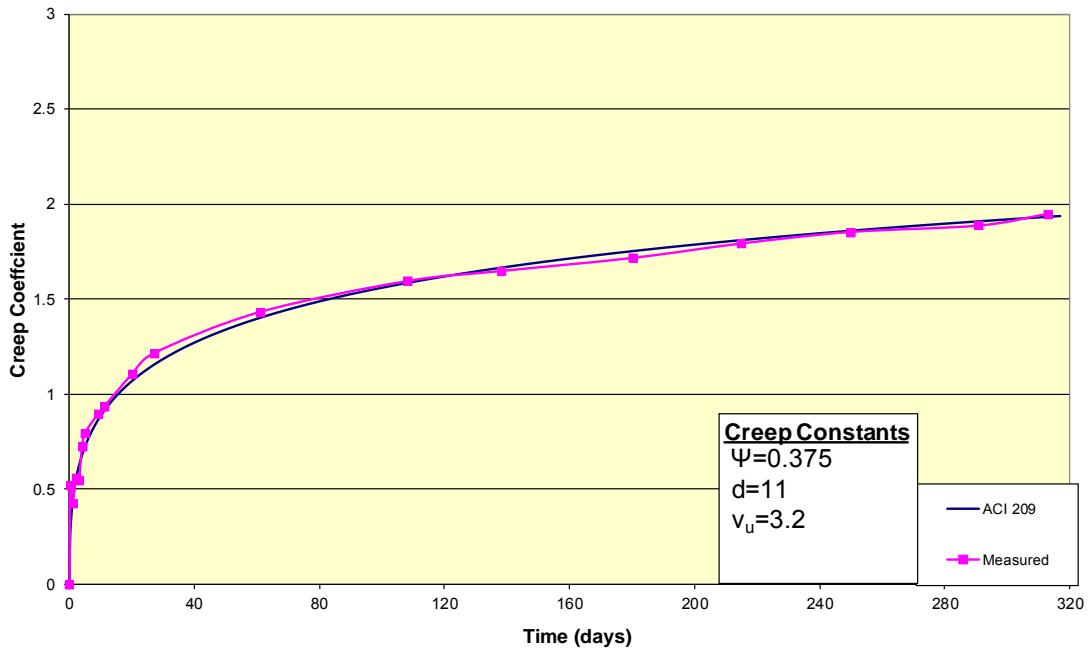


FIGURE 6.3
Creep Coefficient of T-Day #2

T-Day Creep Ratio #3

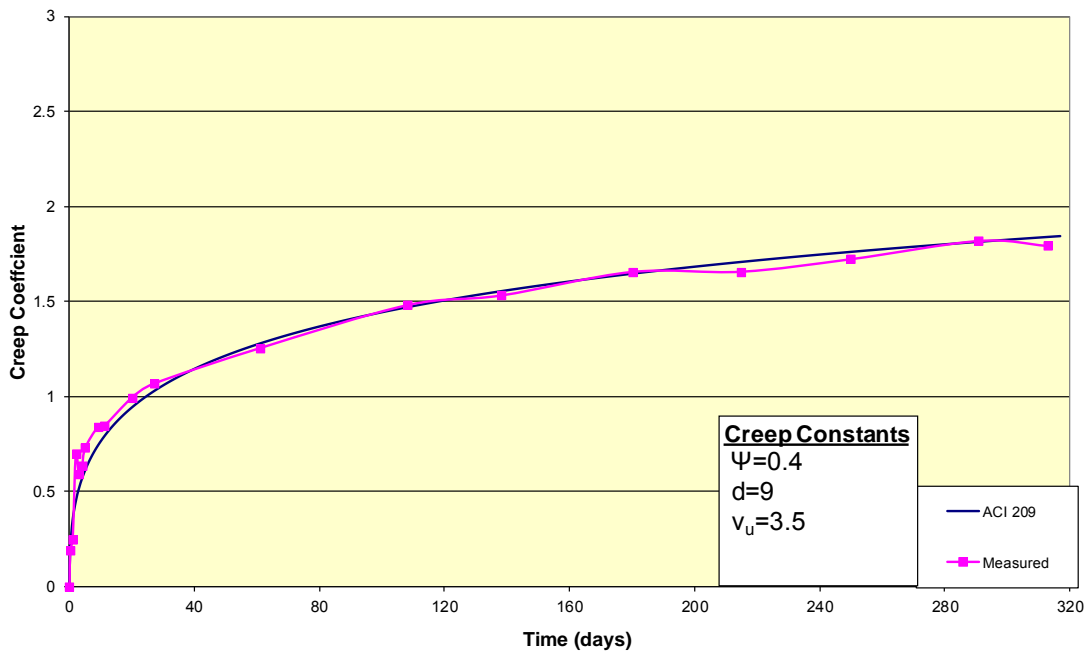


FIGURE 6.4
Creep Coefficient of T-Day #3

28-Day Creep Ratio #1

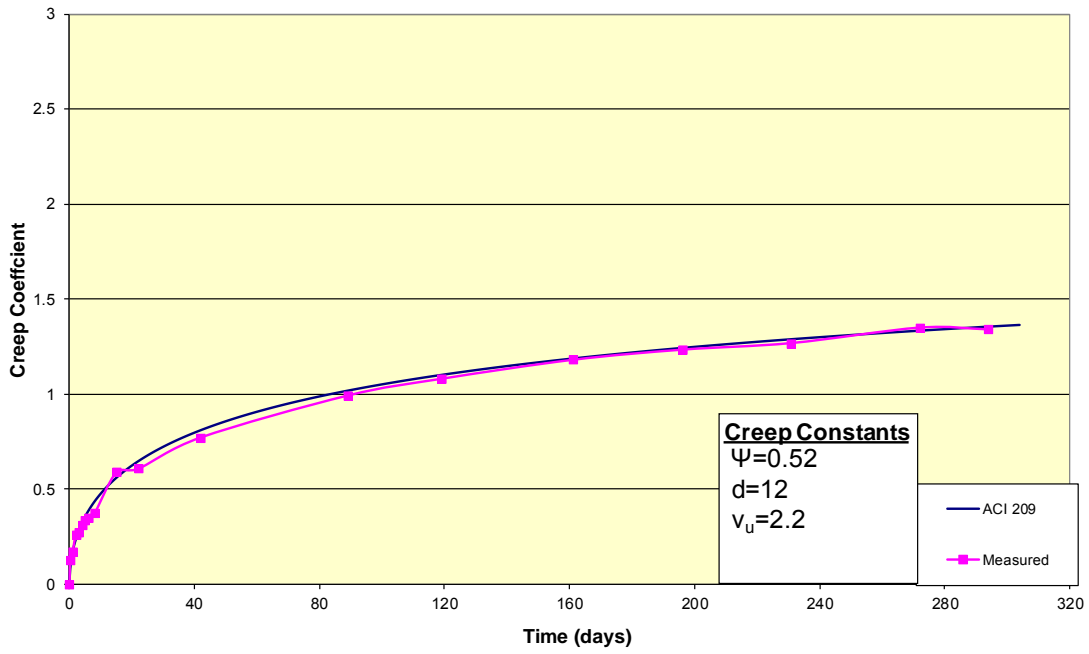


FIGURE 6.5
Creep Coefficient of 28-Day #1

28-Day Creep Ratio #2

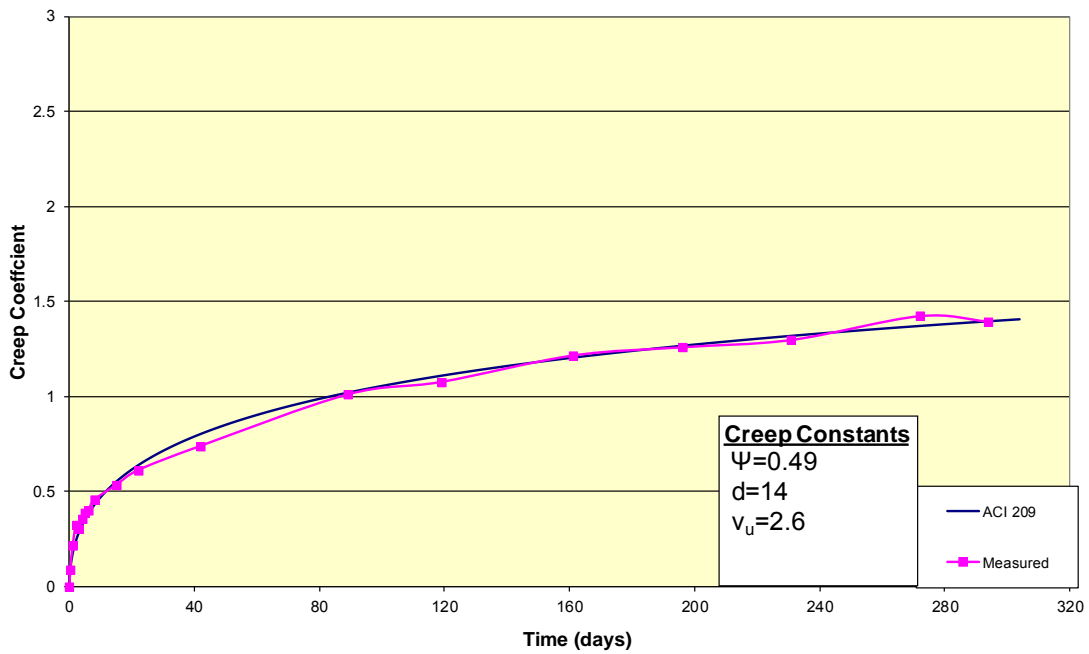


FIGURE 6.6
Creep Coefficient of 28-Day #2

28-Day Creep Ratio #3

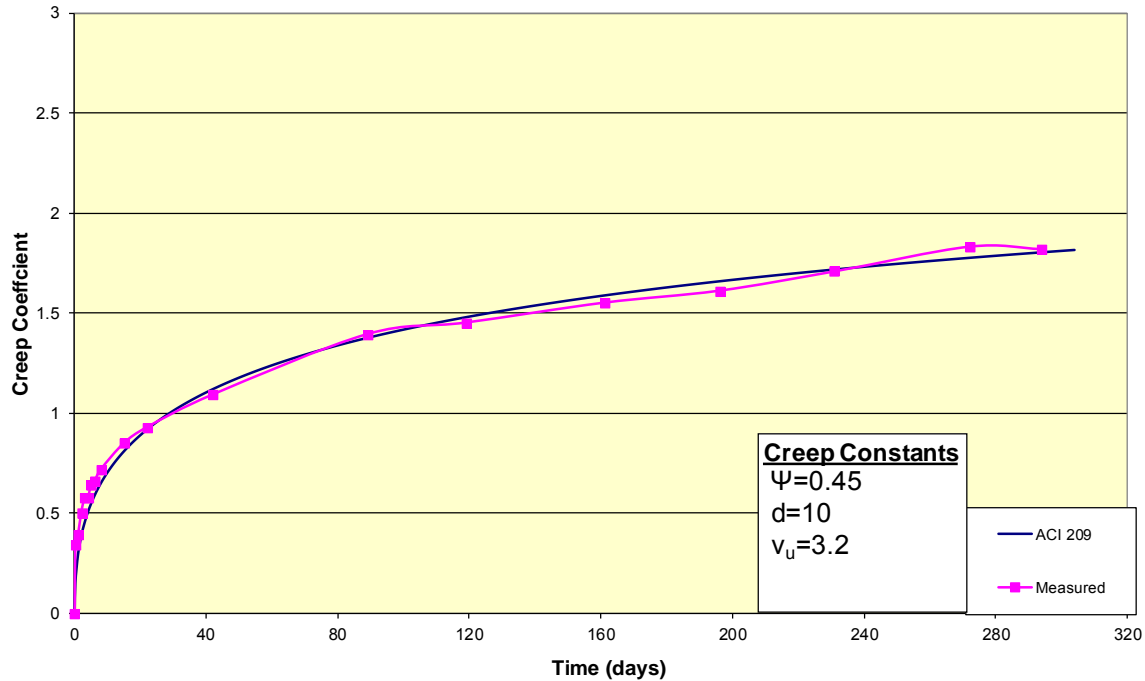


FIGURE 6.7
Creep Coefficient of 28-Day #3

TABLE 6.1
Summary of Creep and Shrinkage Parameters

Parameters		Transfer Day #1	Transfer Day #2	Transfer Day #3	Average T-Day	28 Day #1	28 Day #2	28 Day #3	Average 28 Day
Creep	ψ	0.52	0.375	0.4	0.43	0.52	0.49	0.45	0.49
	d	6	11	9	8.7	12	14	10	12.0
	v_u	3.4	3.2	3.5	3.4	2.2	2.6	3.2	2.7
Shrinkage	f	40	40	40	40.0	30	40	45	38.3
	α	1.05	0.9	1.1	1.0	0.95	0.9	1	1.0
	$(\epsilon_{sh})_u$	450	625	500	525	500	500	425	475

6.4 Shrinkage Results

Shrinkage readings were taken at the same time as the creep readings. The measured strain readings were compared to calculated values from ACI Committee 209 (2005) for each set of specimens. Using Equation 6.2, variables α , f , and $(\epsilon_{sh})_u$ were changed until the fit data resembled the experimental shrinkage data. Figures 6.8-6.10 show shrinkage results from the first prisms that were matched with the T-Day creep prisms. Figures 6.11-6.13 show shrinkage

results from the set of prisms matched with the 28-Day creep prisms. Shrinkage parameters for both sets of specimens are summarized in Table 6.1.

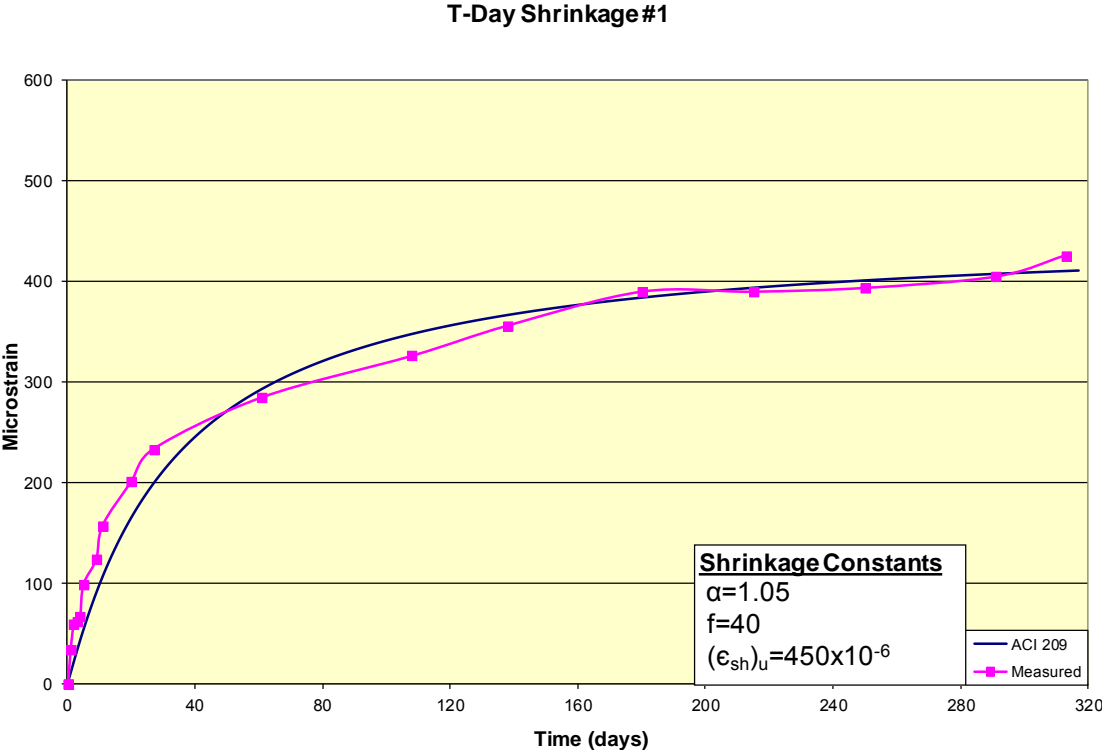


FIGURE 6.8
Shrinkage Strains from T-Day #1

T-Day Shrinkage #2

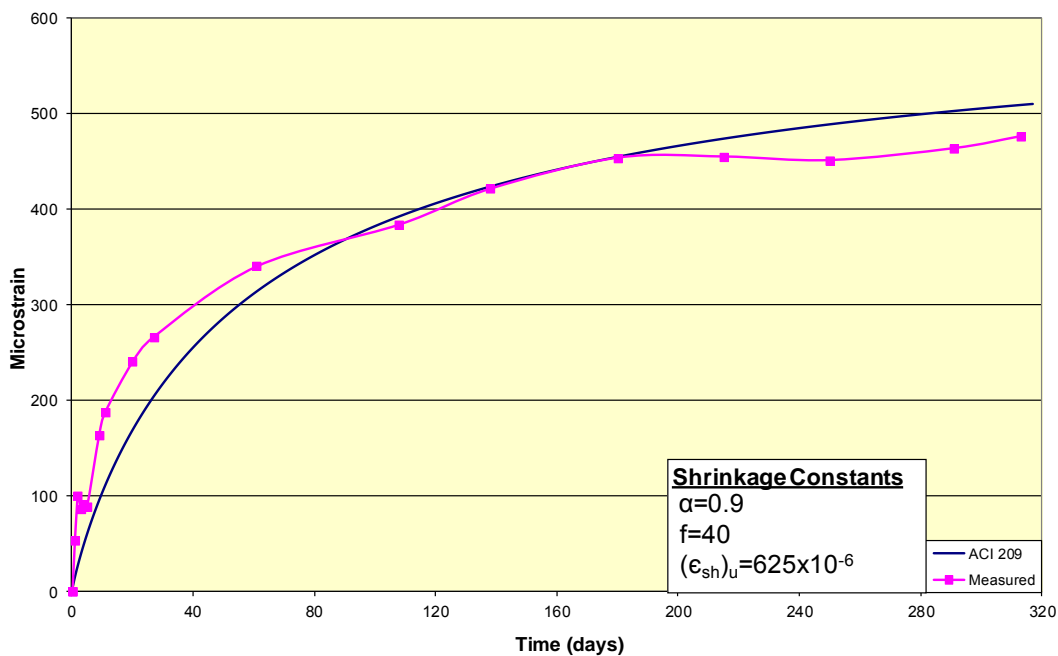


FIGURE 6.9
Shrinkage Strains from T-Day #2

T-Day Shrinkage #3

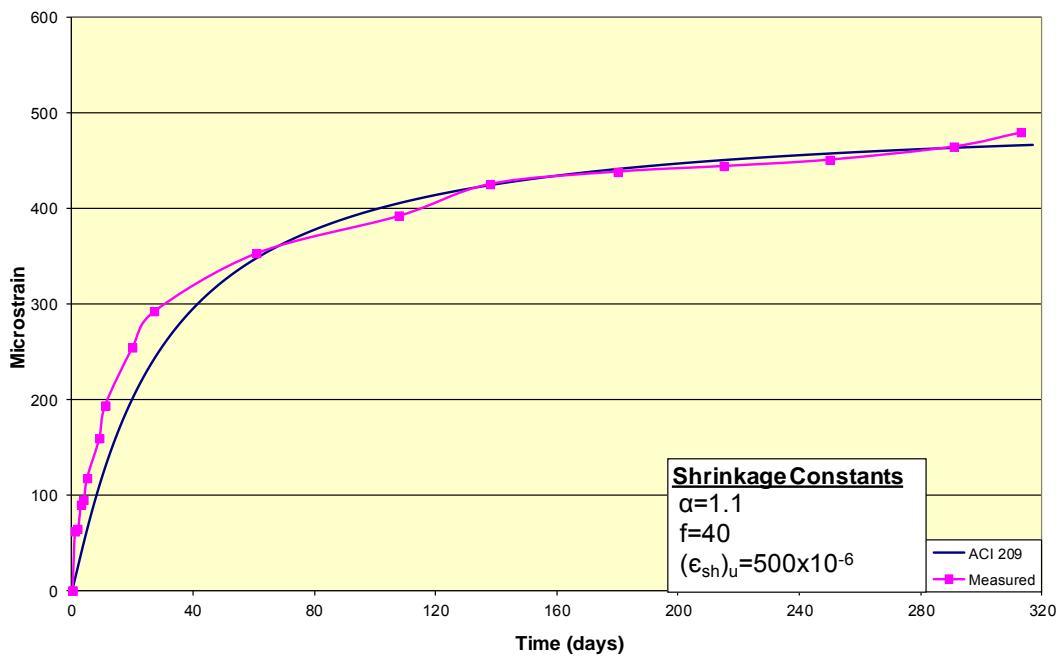


FIGURE 6.10
Shrinkage Strains from T-Day #3

28-Day Shrinkage #1

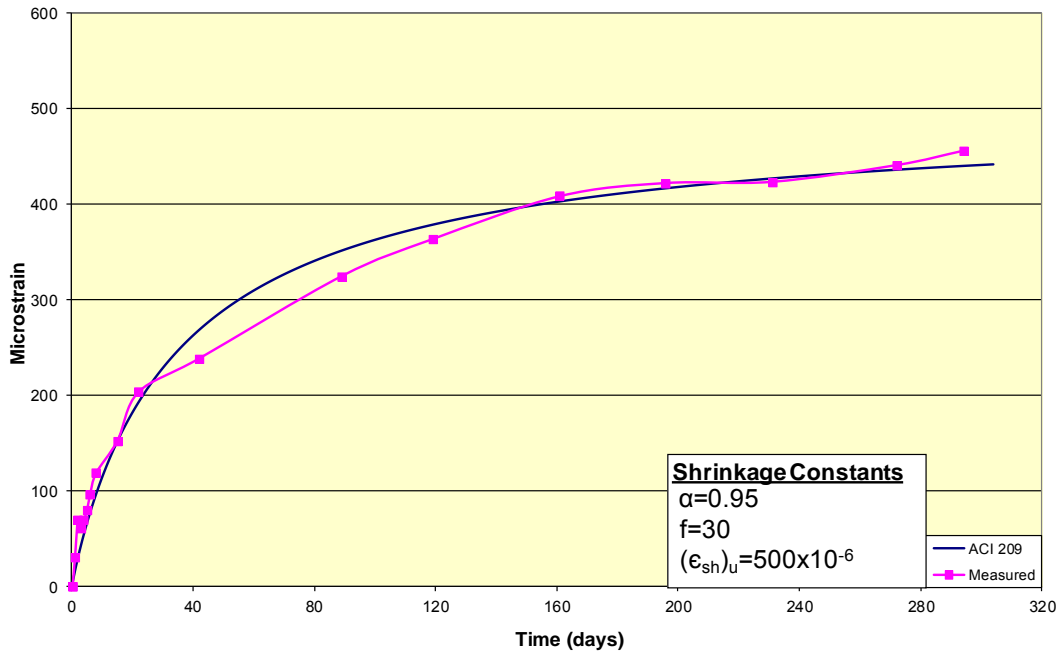


FIGURE 6.11
Shrinkage Strains from 28-Day #1

28-Day Shrinkage #2

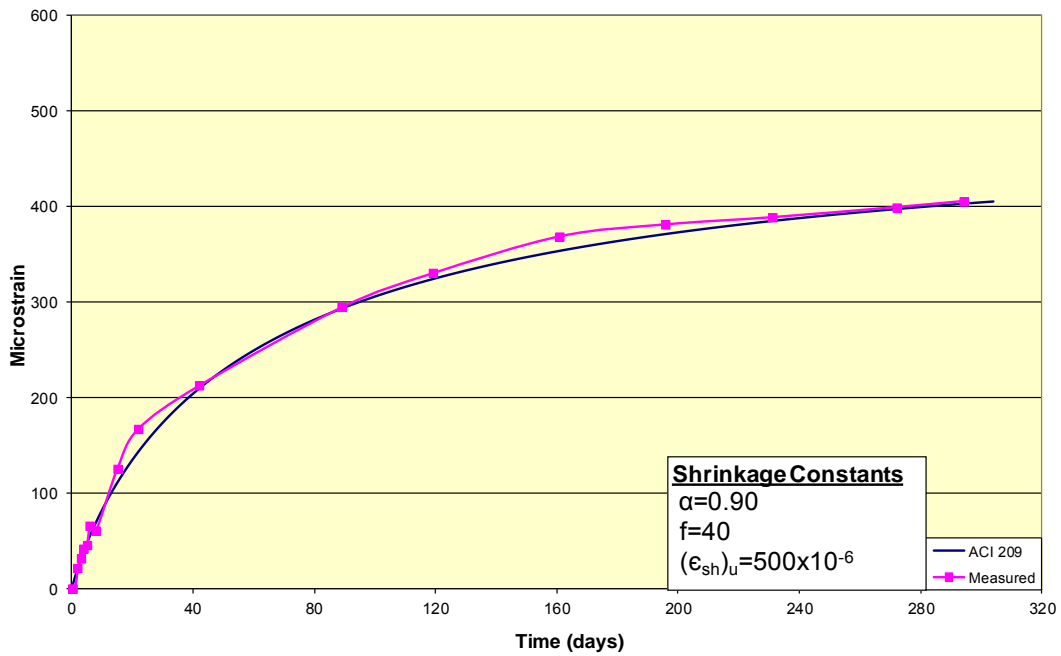


FIGURE 6.12
Shrinkage Strains from 28-Day #2

28-Day Shrinkage #3

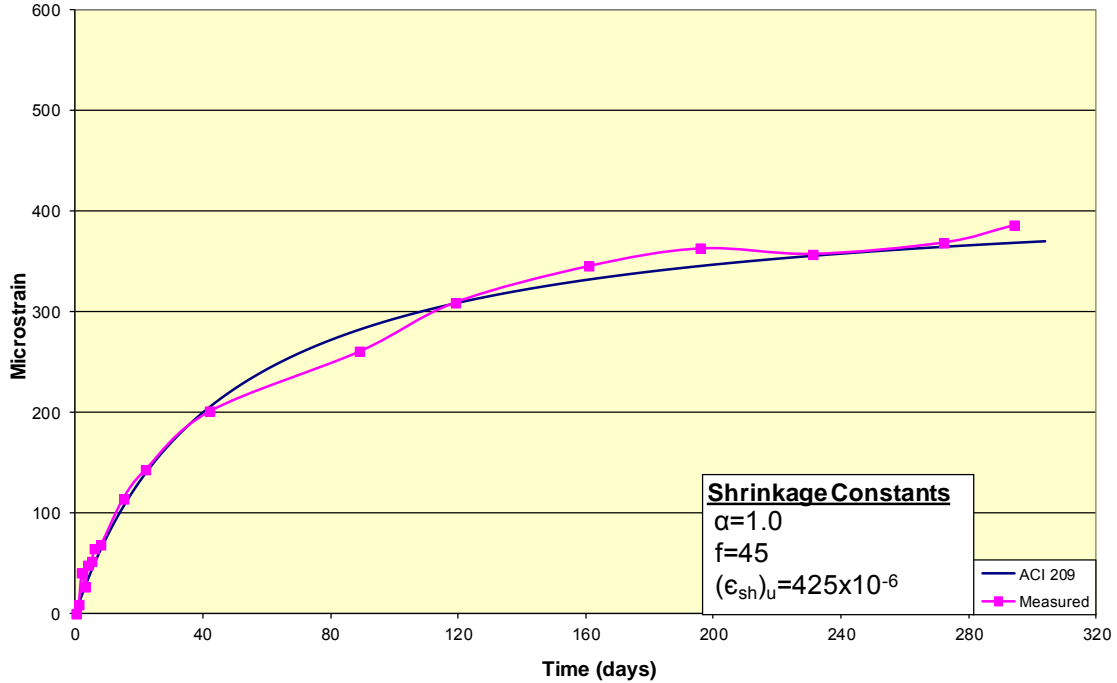


FIGURE 6.13
Shrinkage Strains from 28-Day #3

6.5 ACI 209 Prestress Loss Summary

ACI Committee 209 has a method for predicting prestress losses based on parameters found from creep and shrinkage prisms. The equations used for these losses use the creep coefficient and the ultimate shrinkage strains to predict the long term losses. The calculations of these losses can be seen in Appendix B. Table 6.2 shows a summary of the ACI 209 predicted losses.

TABLE 6.2
Summary of ACI 209 Losses

ACI 209 Method	Elastic Shortening	Creep	Shrinkage	Relaxation	Effective Prestress
Spans 1 and 2	17.4	40.9	10.9	5.06	128
Span 3	20.8	48.9	10.7	5.06	117

**All values in ksi*

Chapter 7: Conclusions and Recommendations

This study on monitoring the system as described in this report, provided beneficial data and findings that are useful for future research on the subject. Creep and shrinkage prisms provided data to predict long term creep and shrinkage of the concrete mix that was used for the girders in this study. The vibrating wire strain gages provided critical data in this study.

1. The method used for instrumenting the girders was well planned, leading to useful data. It provided a good method of instrumenting the girders while keeping the instruments safe and out of the elements. The remote access using the modem was very beneficial while working properly. A larger solar panel and battery provided a reliable source of power while using the modem. The data logger worked well without having the modem connected and only had one power issue when the battery became old and failed.
2. The creep and shrinkage prisms were beneficial in providing useful parameters. These parameters provided larger prestress losses than were measured in the girder. The difference in size between the prisms and girder could have caused this difference in loss calculations even though the volume to surface ratio was corrected for. Another possible cause for the difference in loss predictions could be the amount of force the prisms were loaded to versus the girder's prestress force.
3. The data provided by the vibrating wire strain gages provided important information about the girders' behaviors. The mid spans of the three girders were found to act linear and elastic throughout the study, following the classical beam theory of plane-remaining-plane after deformation. The end locations that were monitored showed a different behavior immediately after loading and kept this behavior throughout the study. This behavior is consistent with the Saint-Venant theory, where the state of stress distribution is not classical at the immediate locations of the points of application of concentrated loads; here, the prestressing forces exerted at the ends of the girders. The vibrating wire strain gages provided

an accurate measurement of the effective prestress in the girders. The code equations were shown to provide higher amounts of losses than those that were found in the girders. So, all of the code equations predicted a higher loss value compared to the experimental measurements during the monitoring phase of this study.

Results of this study serve as one of the many studies required to reach a solid conclusion. Compilation of these studies will provide reliable conclusions that can be considered in possible changes in AASHTO specifications. This compilation can be done by AASHTO or preferably, by KDOT in terms of a project that will be done to conduct a detailed/comprehensive literature review and in-depth study of all the related work, including the current study. The final report of the proposed study will then pave the way for necessary modifications not only by KDOT (in their specifications) but also AASHTO. However, before such a study, the current AASHTO and pertinent KDOT specifications can be used.

References

- AASHTO. 2004. "LRFD Bridge Design Specifications." American Association of State Highway and Transportation Officials.
- ACI Committee 209. 2005. Report on Factors Affecting Shrinkage and Creep of Hardened Concrete, ACI 209.1R-05, American Concrete Institute.
- ACI Committee 318. 2008. Building Code Requirements for Structural Concrete, 318-08, American Concrete Institute.
- ASTM C31. 2009. Standard Practice for Making and Curing Concrete Test Specimens in the Field.
- ASTM C39. 2009. Standard Test Method for Compressive Strength of Cylindrical Concrete Specimens.
- ASTM C138. 2009. Standard Test Method for Density, Yield, and Air Content (Gravimetric) of Concrete.
- ASTM C173. 2009. Standard Test Method for Air Content of Freshly Mixed Concrete by the Volumetric Method.
- ASTM C192. 2009. Standard Practice for Making and Curing Concrete Test Specimens in the Laboratory.
- ASTM C512. 2009. Standard Test Method for Creep of Concrete in Compression.
- ASTM C1611. 2009. Standard Test Method for Slump Flow of Self-Consolidating Concrete.
- ASTM C1621. 2009. Standard Test Method for Passing Ability of Self-Consolidating Concrete by J-Ring.
- Barnes, R.W., J. W. Grove, and N. H. Burns. 2003. "Experimental Assessment Factors Affecting Transfer Length." *ACI Structural Journal* 100 (6): 740–748.
- Buckner, D. 1995. "A Review of Strand Development Length for Pretensioned Concrete Members." *PCI Journal* 40 (2): 84–105.
- Girgis, A.F.M., and C. Y. Tuan. 2005. "Bond Strength and Transfer Length of Pretensioned Bridge Girders Cast with Self-Consolidating Concrete." *PCI Journal* 50 (6): 72–87.
- Google Maps. 2013. <https://maps.google.com/maps?hl=en&tab=wl>.
- Holste, J.R. 2010. "Evaluating Time-Dependent and Bond Characteristics of a Lightweight Concrete Mix for Kansas Prestressed Concrete Bridges." Kansas State University.

- Khayat, K.H., J. Assaad, and J. Daczko. 2004. "Comparison of Field-Oriented Test Methods to Assess Dynamic Stability of Self-Consolidating Concrete." *ACI Materials Journal* 101 (2): 168–176.
- Larson, K.H. 2006. "Evaluating the Time-Dependent Deformations and Bond Characteristics of a Self-Consolidating Concrete Mix and the Implication for Pretensioned Bridge Applications." Kansas State University.
- Larson, K.H., R. J. Peterman, and A. Esmaeily. 2007. "Bond Characteristics of Self-Consolidating Concrete for Prestressed Bridge Girders." *PCI Journal* 52 (4): 44–57.
- Logan, D. R. 1997. "Acceptance Criteria for Bond Quality of Strand for Pretensioned Prestressed Concrete Applications." *PCI Journal* 42 (2): 52–90.
- Moustafa, S. 1974. "Pull-Out Strength of Strand and Lifting Loops." Concrete Technology Associates Technical Bulletin 74-B5.
- Ouchi, M. 2001. "Self-Compacting Concrete Development, Applications and Investigations." *Proceedings of the Fourth International Conference on Materials Engineering for Resources 1*: 53–58.
- PCI Industry Handbook Committee. 2004. *PCI Design Handbook, Sixth Edition*. Chicago, IL, Precast/Prestress Concrete Institute.
- Peterman, R.J. 2007. "Effects of As-Cast Depth and Concrete Fluidity on Strand Bond." *PCI Journal* 52 (3): 72–101.
- Russell, B.W., and N. H. Burns. 1996. "Measured Transfer Lengths of 0.5-in. and 0.6-in. Strands in Pretensioned Concrete." *PCI Journal* 41 (5): 44–65.
- Shing, P.B., D. M. Frangopol, M. L. McMullen, W. Hutter, D. E. Cooke, and M. A. Leonard. 2000. "Strand Development and Transfer Length Tests on High-Performance Concrete Box Girders." *PCI Journal* 45 (5): 96–109.
- Steinberg, E., J. T. Beier, and S. Sargand. 2001. "Effects of Sudden Prestress Force Transfer in Pretensioned Concrete Beams." *PCI Journal* 46 (1): 64–75.
- Weerasekera, I.R.A., A. Sabesh, and R. E. Loov. 2008. "Reliability of Bond Measuring Devices in Pretensioned Prestressed Concrete." *Innovations in Structural Engineering and Construction 1*: 333–338.

DATE 7-Apr-10

TECHNICIAN SY,JI,BC,JA

TRUCK NO.	BED NO.	MIX NO.	CU. YDS	TIME	TEMP AMB	CON	UNIT WT.	% AIR	INITIAL DIA. IN.	J RING	T Time	VSI	# ADMIX ADDED	INITIAL DIA. IN.	J RING	T Time	VSI	
235	1514	9058	10.00	11:14	40	55	35.2	7.2	24 1/2	23	0	0	2 1/2	28			0	
276	1514	9058	10.00	11:33	40	56	35.4	6.9	24		0	0	1 1/2	27			0	
234	1514	9058	10.00	11:43	40	64	35.5	6.8	24 1/2		0	0	1 1/2	27 1/2			0	
231	1514	9058	10.00	11:57	40	67	35.7	7.5	25	24	0	0	1	26 1/2			0	
235	1514	9058	10.00	12:00	40	68	35.8	7.1	26		0	0						
276	1514	9058	6.25	12:15	40	68	35.9	6.8	26 1/2		0	0						
Release brakes on pour # 39																		
load 1																		
5920																		
Average:6056																		

Visual Index No's: 0 - No evidence of segregation in slump flow patty or in mixer drum or wheelbarrow.
 1 - No mortar halo or aggregate pile in the slump flow patty but some slight bleed or air popping on the surface of the concrete in the mixer drum or wheelbarrow.
 2 - A slight mortar halo (<10mm) and/or aggregate pile in the slump flow patty and highly noticeable bleeding in the mixer drum and wheelbarrow.
 3 - Clearly segregating by evidence of a large mortar halo (>10mm) and/or a large aggregate pile in the center of the concrete patty and a thick layer of paste on the surface of the resting concrete in the mixer drum or wheelbarrow.

Low Slump Balls A - No low slump balls B - Slump balls under 1" dia C - Slump balls 1" to 2" diameter D - Slump balls larger than 2" diameter

NOTES: Unless noted otherwise admixture added will be Glenium 3400 for gray concrete and Glenium 7700 for white concrete. "Gal" = water added.

FIGURE A.2
Span 2 Mix Properties (Courtesy Ready Mixed Concrete)

Appendix B: Girder Calculations

B.1 Prestress Loss Equations

ACI and PCI Methods

(ACI Committee 318, 2005 and PCI Design Handbook, 2004)

Elastic Shortening of Concrete (ES):

$$ES = K_{es} E_s \frac{f_{cir}}{E_{ci}}$$

where:

K_{es} = 1.0 for pretensioned members

E_{ci} = modulus of elasticity of concrete at time prestress is applied

E_s = modulus of elasticity of prestressing tendons

$$f_{cir} = K_{cir} f_{cpi} - f_g$$

where:

K_{cir} = 0.9 for pretensioned members

Creep of Concrete (CR):

Members with bonded tendons:

$$CR = K_{cr} \frac{E_s}{E_c} \times [f_{cir} - f_{cfs}]$$

where:

K_{cr} = 2.0 for normal weight concrete

Shrinkage of Concrete (SH):

$$SH = (8.2 \times 10^{-6}) \times K_{sh} \times E_{ps} \times \left[1 - 0.06 \times \frac{V}{S} \right] \times [100 - RH]$$

where:

K_{sh} = 1.0 for pretensioned members

V/S= volume-to-surface ratio

RH= average ambient relative humidity

Relaxation of Tendons (RE):

$$RE = [K_{re} - J \times (SH + CR + ES)] \times C$$

where:

K_{re} , J , and C are taken from tables in PCI Handbook (2004)

AASHTO Method

From Third Edition AASHTO (2004)

$$\Delta f_{pT} = \Delta f_{pES} + \Delta f_{pSR} + \Delta f_{pCR} + \Delta f_{pR2}$$

where:

Δf_{pT} = total loss (ksi)

Δf_{pES} = loss due to elastic shortening (ksi)

Δf_{pSR} = loss due to shrinkage (ksi)

Δf_{pCR} = loss due to creep of concrete (ksi)

Δf_{pR2} = loss due to relaxation of steel after transfer (ksi)

Elastic Shortening (Δf_{pES}):

$$\Delta f_{pES} = \frac{E_p}{E_{ci}} \times f_{cgp}$$

where:

f_{cgp} = sum of stresses in concrete at the center of gravity of the prestressing tendons due to the prestressing force at transfer and the self-weight of the member at the section of maximum moment (ksi)

E_p = modulus of elasticity of prestressing steel (ksi)

E_{ci} = modulus of elasticity of concrete at transfer (ksi)

Shrinkage (Δf_{pSR}):

$$\Delta f_{pSR} = [17.0 - 0.150 \times H]$$

where:

H = average annual ambient relative humidity

Creep (Δf_{pCR}):

$$\Delta f_{pCR} = 12.0 \times f_{cgp} - 7.0 \times \Delta f_{cdp} \geq 0$$

where:

f_{cgp} = concrete stress at center of gravity of prestressing steel at transfer

Δf_{cdp} = change in concrete stress at center of gravity of prestressing steel due to permanent loads with the exception of the load acting at the time the prestressing force is applied. Values of Δf_{cdp} should be calculated at the same section or at sections at which f_{cgp} is calculated (ksi)

Relaxation (Δf_{pR2}):

$$\Delta f_{pR2} = 20.0 - 0.4 \times \Delta f_{pES} - 0.2 \times [\Delta f_{pSR} + \Delta f_{pCR}]$$

where:

Δf_{pES} = loss due to elastic shortening (ksi)

Δf_{pSR} = loss due to shrinkage (ksi)

Δf_{pCR} = loss due to creep of concrete (ksi)

B.2 Prestress Loss Calculations for Spans 1 and 2

ACI and PCI Methods

Elastic Shortening of Concrete (ES):

$$ES = K_{es} E_s \frac{f_{cir}}{E_{ci}}$$

K_{es} = 1.0 for pretensioned members

$$E_{ci} = 33w^{1.5} \sqrt{f'_c} = 33 \times 155^{1.5} \times \sqrt{6000} = 4933 \text{ksi (ACI 318 2008)}$$

E_s = 28,500 ksi

$$f_{cir} = K_{cir} f_{cpi} - f_g$$

K_{cir} = 0.9 for pretensioned members

$$f_{cir} = 0.9 \times \left[\frac{1581}{903.8} + \frac{1581 \times 32.37^2}{790592} \right] - \frac{1695 \times 12 \times 32.37}{790592} = 2.63 \text{ksi}$$

$$ES = 1 \times 28500 \times \frac{2.63}{4933} = 15.19 \text{ksi}$$

Creep of Concrete (CR):

$$CR = K_{cr} \frac{E_s}{E_c} \times [f_{cir} - f_{cds}]$$

$K_{cr} = 2.0$ for normal weight concrete

$$f_{cds} = 0.919 \text{ksi}$$

$$CR = 2.0 \times \left[\frac{28500}{5871} \right] \times (2.63 - 0.919) = 16.61 \text{ksi}$$

Shrinkage of Concrete (SH):

$$SH = (8.2 \times 10^{-6}) \times K_{sh} \times E_{ps} \times \left[1 - 0.06 \times \frac{V}{S} \right] \times [100 - RH]$$

$K_{sh} = 1.0$ for pretensioned members

$$V/S = 2.9$$

$RH = 70\%$

$$SH = (8.2 \times 10^{-6}) \times 1 \times 28500 \times [1 - 0.06 \times 2.9] \times [100 - 70] = 5.79 \text{ksi}$$

Relaxation of Tendons (RE):

$$RE = [K_{re} - J \times (SH + CR + ES)] \times C$$

$$K_{re} = 5.0$$

$$J = 0.04$$

$$C = 1.0$$

$$RE_L = [5 - 0.04 \times (15.19 + 16.61 + 5.79)] \times 1 = 3.50 \text{ksi}$$

Total Losses:

$$TL = 15.19 + 16.61 + 5.79 + 3.50 = 41.09$$

$$f_{se} = f_{pj} - TL = 202.5 - 41.09 \approx 161 \text{ksi}$$

AASHTO Method

$$\Delta f_{pT} = \Delta f_{pES} + \Delta f_{pSR} + \Delta f_{pCR} + \Delta f_{pR2}$$

Elastic Shortening (Δf_{pES}):

$$\Delta f_{pES} = \frac{E_p}{E_{ci}} \times f_{cgp}$$

$$f_{cgp} = \left[\frac{1581}{903.8} + \frac{1581 \times 32.37^2}{790592} \right] - \frac{1695 \times 12 \times 32.37}{790592} = 3.01 \text{ksi}$$

$$\Delta f_{pES} = \frac{28500}{4933} \times 3.01 = 17.4 \text{ksi}$$

Shrinkage (Δf_{pSR}):

$$\Delta f_{pSR} = [17.0 - 0.150 \times 70] = 6.5 \text{ksi}$$

Creep (Δf_{pCR}):

$$\Delta f_{pCR} = 12.0 \times 3.01 - 7.0 \times 0.83 \geq 0$$

$$\Delta f_{pCR} = 30.31 \text{ksi}$$

Relaxation (Δf_{pR2}):

$$\Delta f_{pR2} = \{20.0 - 0.4 \times 17.4 - 0.2 \times [6.5 + 30.31]\} \times 0.3 = 1.7 \text{ksi}$$

Total Losses

$$\Delta f_{pT} = 17.4 + 6.5 + 30.31 + 1.7 = 55.91 \text{ksi}$$

$$f_{se} = 202.5 - 55.91 = 146.59 \text{ksi}$$

B.3 Prestress Loss Calculations for Span 3

ACI and PCI Methods

Elastic Shortening of Concrete (ES):

$$ES = K_{es} E_s \frac{f_{cir}}{E_{ci}}$$

$$K_{es} = 1.0 \text{ for pretensioned members}$$

$$E_{ci} = 33w^{1.5} \sqrt{f'_c} = 33 \times 155^{1.5} \times \sqrt{6000} = 4933 \text{ksi (ACI 318 2008)}$$

$$E_s = 28,500 \text{ ksi}$$

$$f_{cir} = K_{cir} f_{cpi} - f_g$$

$$K_{cir} = 0.9 \text{ for pretensioned members}$$

$$f_{cir} = 0.9 \times \left[\frac{1933.5}{903.8} + \frac{1933.5 \times 31.61^2}{790592} \right] - \frac{2050 \times 12 \times 31.61}{790592} = 3.14 \text{ksi}$$

$$ES = 1 \times 28500 \times \frac{3.14}{4933} = 18.14 \text{ksi}$$

Creep of Concrete (CR):

$$CR = K_{cr} \frac{E_s}{E_c} \times [f_{cir} - f_{cds}]$$

$$K_{cr} = 2.0 \text{ for normal weight concrete}$$

$$f_{cds} = 1.087 \text{ksi}$$

$$CR = 2.0 \times \left[\frac{28500}{5871} \right] \times (3.14 - 1.087) = 19.93 \text{ksi}$$

Shrinkage of Concrete (SH):

$$SH = (8.2 \times 10^{-6}) \times K_{sh} \times E_{ps} \times \left[1 - 0.06 \times \frac{V}{S} \right] \times [100 - RH]$$

$$K_{sh} = 1.0 \text{ for pretensioned members}$$

$$V/S = 2.9$$

$$RH = 70\%$$

$$SH = (8.2 \times 10^{-6}) \times 1 \times 28500 \times [1 - 0.06 \times 2.9] \times [100 - 70] = 5.79 \text{ksi}$$

Relaxation of Tendons (RE):

$$RE = [K_{re} - J \times (SH + CR + ES)] \times C$$

$$K_{re} = 5.0$$

$$J = 0.04$$

$$C = 1.0$$

$$RE_L = [5 - 0.04 \times (18.14 + 19.92 + 5.79)] \times 1 = 3.25 \text{ksi}$$

Total Losses:

$$TL = 18.14 + 19.92 + 5.79 + 3.25 = 47.1$$

$$f_{se} = f_{pj} - TL = 202.5 - 47.1 \approx 155 \text{ksi}$$

AASHTO Method

$$\Delta f_{pT} = \Delta f_{pES} + \Delta f_{pSR} + \Delta f_{pCR} + \Delta f_{pR2}$$

Elastic Shortening (Δf_{pES}):

$$\Delta f_{pES} = \frac{E_p}{E_{ci}} \times f_{cgp}$$

$$f_{cgp} = \left[\frac{1933.5}{903.8} + \frac{1933.5 \times 31.61^2}{790592} \right] - \frac{2050 \times 12 \times 31.61}{790592} = 3.60 \text{ksi}$$

$$\Delta f_{pES} = \frac{28500}{4933} \times 3.60 = 20.8 \text{ksi}$$

Shrinkage (Δf_{pSR}):

$$\Delta f_{pSR} = [17.0 - 0.150 \times 70] = 6.5 \text{ksi}$$

Creep (Δf_{pCR}):

$$\Delta f_{pCR} = 12.0 \times 3.6 - 7.0 \times 0.98 \geq 0$$

$$\Delta f_{pCR} = 36.34 \text{ksi}$$

Relaxation (Δf_{pR2}):

$$\Delta f_{pR2} = \{20.0 - 0.4 \times 20.8 - 0.2 \times [6.5 + 36.34]\} \times 0.3 = 0.9 \text{ksi}$$

Total Losses

$$\Delta f_{pT} = 20.8 + 6.5 + 36.34 + 0.9 = 64.54 \text{ksi}$$

$$f_{se} = 202.5 - 64.54 = 137.96 \text{ksi}$$

B.4 ACI 209 Prestress Loss Equations and Calculations

$$\lambda_u = \left[(nf_c) + (nf_c)v_u \left(1 - \frac{F_u}{2F_o} \right) + \frac{(\varepsilon_{SH})_u E_s}{(1 + n\rho\xi_s)} + (f_{sr})_u \right]$$

where:

λ_u = total losses in ksi

n = modular ratio, E_s/E_c , at the time of loading

f_c = concrete stress such as at steel c.g.s due to prestress and precast beam dead load

v_u = ultimate creep coefficient

F_u = total ultimate (in time) loss of prestress minus the initial elastic loss

F_o = prestress force at transfer, after elastic loss

$(\varepsilon_{SH})_u$ = ultimate (in time) shrinkage strain in (in./in.)

E_s = modulus of elasticity of steel

ρ = reinforcement ratio

ξ_s = cross section shape coefficient

$(f_{sr})_u$ = ultimate (in time) stress loss due to steel relaxation on prestressed members

Span 1 and 2

Elastic shortening:

$$ES = nf_c$$

$$n = \frac{28500}{4933} = 5.73$$

$$f_c = \frac{F_i}{A_t} + \frac{F_i e^2}{I_t} - \frac{M_D e}{I_t}$$

$$f_c = \frac{1581}{903.8} + \frac{1581 * 32.37^2}{790592} - \frac{1695 * 12 * 32.37}{790592} = 3.01 \text{ksi}$$

$$ES = 5.78 * 3.01 = 17.4 \text{ksi}$$

Creep:

$$CR = (nf_c) v_u \left(1 - \frac{F_u}{2F_o} \right)$$

$$n = \frac{28500}{4932} = 5.78$$

$$f_c = 3.01 \text{ksi}$$

$$v_{ui} = 3.4$$

volume to surface correction:

Prisms: $v/s=1$ inch

$$\frac{\lambda_v \text{ prism}}{s} = \text{correction factor for } v/s \text{ ratio from Table 2.5.5.2 (ACI Committee 209)}$$

Beams: $v/s=2.9$ inch

$$\frac{\lambda_v \text{ beam}}{s} = \text{correction factor for } v/s \text{ ratio from Table 2.5.5.2 (ACI Committee 209)}$$

$$\lambda_v = \frac{\frac{\lambda_v \text{ beam}}{s}}{\frac{\lambda_v \text{ prism}}{s}} = \frac{0.83}{1.09} = 0.76$$

Creep

$$v_u = \text{Creep} \lambda_v * v_{ui} = 2.584$$

$$\frac{F_u}{F_o} = 0.18 \text{ from Table 4.4.1.2 (ACI 209 Committee)}$$

$$CR = (5.78 * 3.01) v_u \left(1 - \frac{0.18}{2} \right) = 40.9 \text{ksi}$$

Shrinkage:

$$SH = \frac{(\varepsilon_{SH})_u E_s}{(1 + n\rho\xi_s)}$$

$$n = 5.78$$

$$E_s = 28500$$

$$\rho = \frac{36 * 0.217}{903.8} = 0.00864$$

$$\xi_s = 1 + \frac{e^2}{r^2} = 1 + \frac{32.37^2}{\left(\frac{790592}{903.8}\right)} = 2.20$$

$$SH = \frac{(\varepsilon_{SH})_u * 28500}{(1 + 5.78 * 0.00864 * 2.20)}$$

volume to surface correction:

Prisms: v/s=1 inch

$$\frac{\lambda_{v,prism}}{s} = \text{correction factor for v/s ratio from Table 2.5.5.2 (ACI Committee 209)}$$

Beams: v/s=2.9 inch

$$\frac{\lambda_{v,beam}}{s} = \text{correction factor for v/s ratio from Table 2.5.5.2 (ACI Committee 209)}$$

$$\lambda_{\frac{v}{s}} = \frac{\frac{\lambda_{v,beam}}{s}}{\frac{\lambda_{v,prism}}{s}} = \frac{0.86}{1.06} = 0.81$$

Shrinkage

$$(\varepsilon_{SH})_u = \text{Shrinkage} \lambda_{\frac{v}{s}} * (\varepsilon_{SH})_{ui} = 525 * 10^{-6} * 0.81 = 425 * 10^{-6}$$

$$SH = 10.9 \text{ksi}$$

Relaxation:

$$RE = (f_{sr})_u$$

$$(f_{sr})_u = 0.025(f_{si}) \text{ from Table 4.4.1.3 (ACI 209 Committee)}$$

$$RE = 0.025 * 202.5 = 5.06 \text{ksi}$$

Total Losses:

$$\lambda_u = 17.4 + 40.9 + 10.9 + 5.09 = 74.29 \text{ksi}$$

Span 3

Elastic shortening:

$$ES = nf_c$$

$$n = \frac{28500}{4933} = 5.73$$

$$f_c = \frac{F_i}{A_i} + \frac{F_i e^2}{I_i} - \frac{M_D e}{I_i}$$

$$f_c = \frac{1933.5}{903.8} + \frac{1933.5 * 31.61^2}{790592} - \frac{2050 * 12 * 31.61}{790592} = 3.6 \text{ksi}$$

$$ES = 5.78 * 3.6 = 20.8 \text{ksi}$$

Creep:

$$CR = (nf_c) v_u \left(1 - \frac{F_u}{2F_o} \right)$$

$$n = \frac{28500}{4932} = 5.78$$

$$f_c = 3.6 \text{ksi}$$

$$v_{ui} = 3.4$$

volume to surface correction:

Prisms: $v/s=1$ inch

$\frac{\lambda_v \text{ prism}}{s}$ = correction factor for v/s ratio from Table 2.5.5.2 (ACI Committee 209)

Beams: $v/s=2.9$ inch

$\frac{\lambda_v \text{ beam}}{s}$ = correction factor for v/s ratio from Table 2.5.5.2 (ACI Committee 209)

$$\lambda_v = \frac{\frac{\lambda_v \text{ beam}}{s}}{\frac{\lambda_v \text{ prism}}{s}} = \frac{0.83}{1.09} = 0.76$$

Creep

$$v_u = Creep \lambda_{\frac{v}{s}} * v_{ui} = 2.584$$

$$\frac{F_u}{F_o} = 0.18 \text{ from Table 4.4.1.2 (ACI 209 Committee)}$$

$$CR = (5.78 * 3.6) v_u \left(1 - \frac{0.18}{2} \right) = 48.9 \text{ ksi}$$

Shrinkage:

$$SH = \frac{(\epsilon_{SH})_u E_s}{(1 + n \rho \xi_s)}$$

$$n = 5.78$$

$$E_s = 28500$$

$$\rho = \frac{44 * 0.217}{903.8} = 0.0106$$

$$\xi_s = 1 + \frac{e^2}{r^2} = 1 + \frac{31.61^2}{\left(\frac{790592}{903.8} \right)} = 2.14$$

$$SH = \frac{(\epsilon_{SH})_u * 28500}{(1 + 5.78 * 0.0106 * 2.14)}$$

volume to surface correction:

Prisms: $v/s = 1$ inch

$$\lambda_{\frac{v}{s} prism} = \text{correction factor for } v/s \text{ ratio from Table 2.5.5.2 (ACI Committee 209)}$$

Beams: $v/s = 2.9$ inch

$$\lambda_{\frac{v}{s} beam} = \text{correction factor for } v/s \text{ ratio from Table 2.5.5.2 (ACI Committee 209)}$$

$$\lambda_{\frac{v}{s}} = \frac{\lambda_{\frac{v}{s} beam}}{\lambda_{\frac{v}{s} prism}} = \frac{0.86}{1.06} = 0.81$$

Shrinkage

$$(\epsilon_{SH})_u = Shrinkage \lambda_{\frac{v}{s}} * (\epsilon_{SH})_{ui} = 525 * 10^{-6} * 0.81 = 425 * 10^{-6}$$

$$SH = 10.7 \text{ ksi}$$

Relaxation:

$$RE = (f_{sr})_u$$

$$(f_{sr})_u = 0.025(f_{si}) \text{ from Table 4.4.1.3 (ACI 209 Committee)}$$

$$RE = 0.025 * 202.5 = 5.06ksi$$

Total Losses:

$$\lambda_u = 20.8 + 48.9 + 10.7 + 5.09 = 85.49ksi$$

Appendix C: Additional Graphs

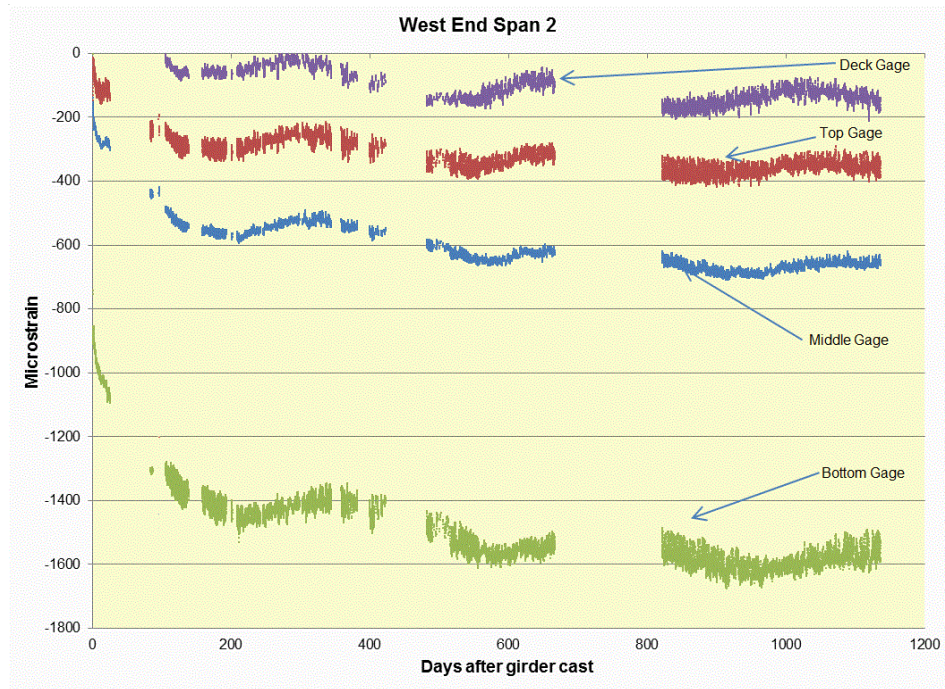


FIGURE C.1
Strain Overtime for Each Gage on West End of Span 2

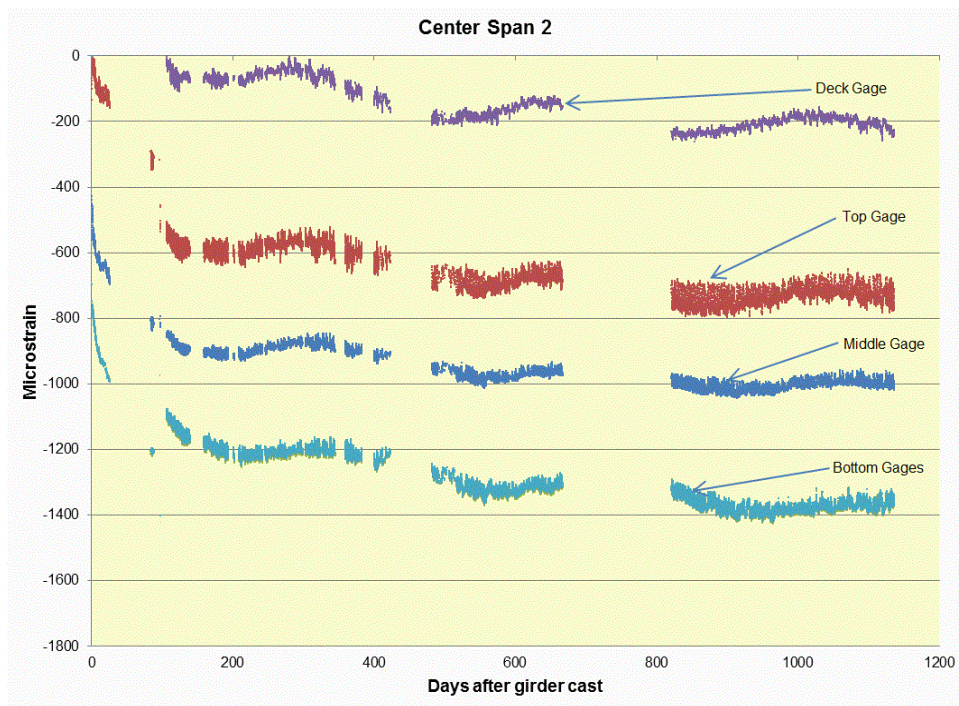


FIGURE C.2
Strain Overtime for Each Gage in Center of Span 2

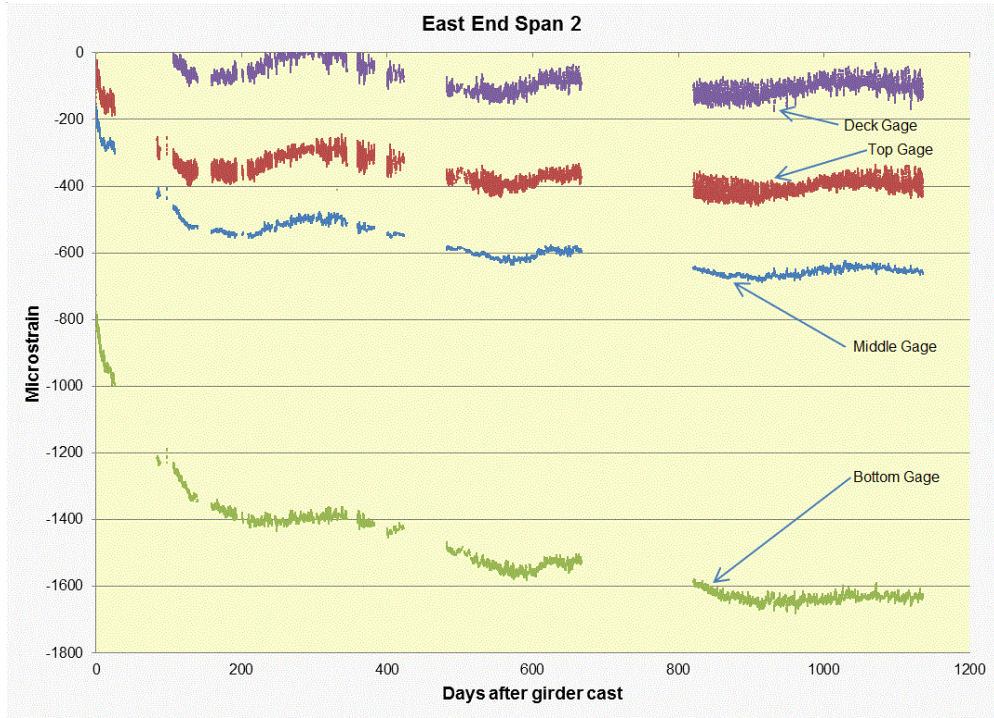


FIGURE C.3
Strain Overtime for Each Gage on East End of Span 2

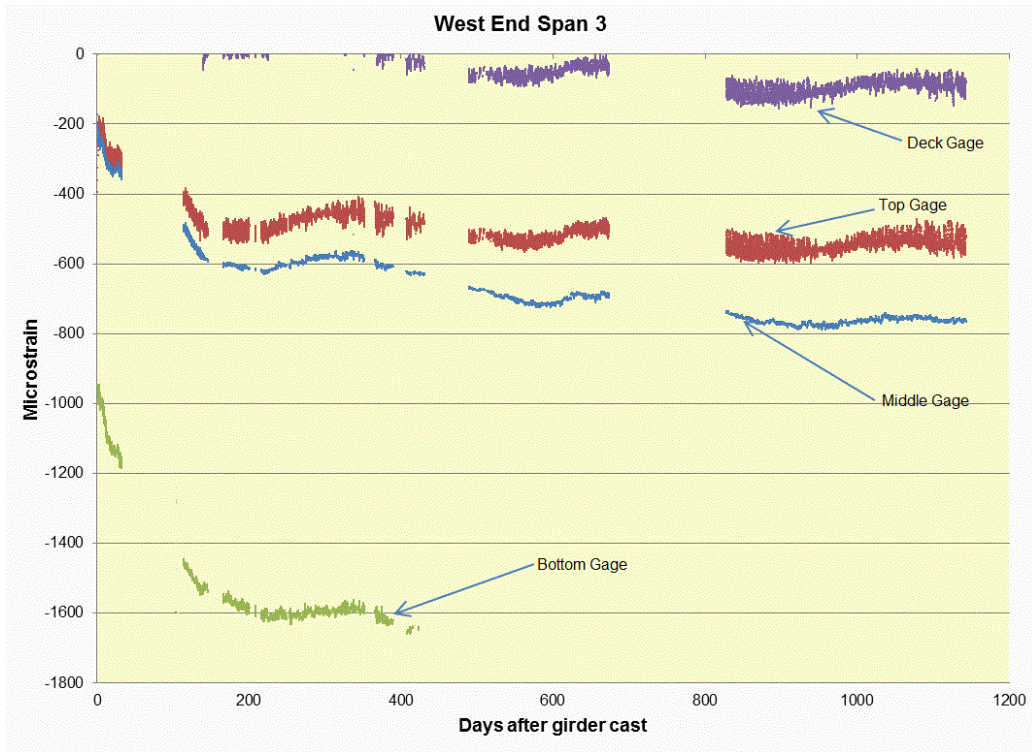


FIGURE C.4
Strain Overtime for Each Gage on West End of Span 3

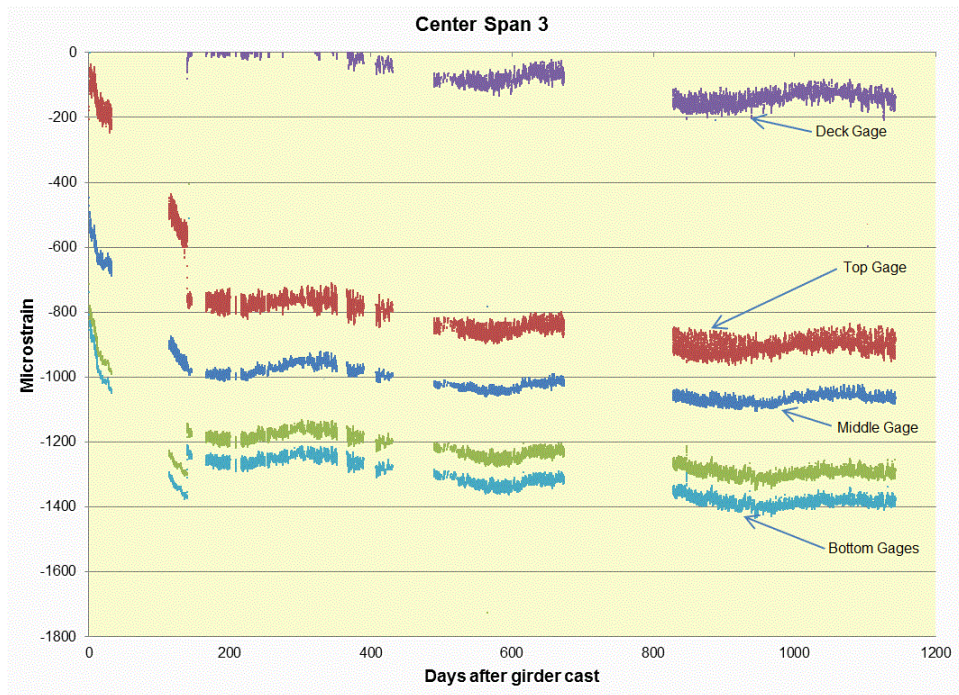


FIGURE C.5
Strain Overtime for Each Gage in Center of Span 3

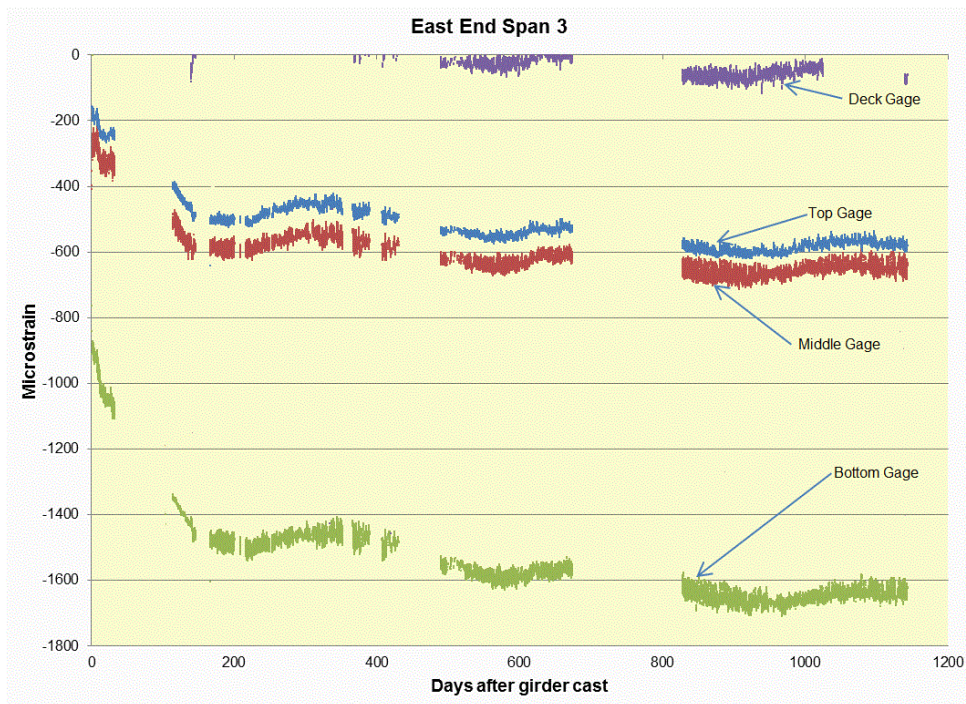


FIGURE C.6
Strain Overtime for Each Gage on East End of Span 3

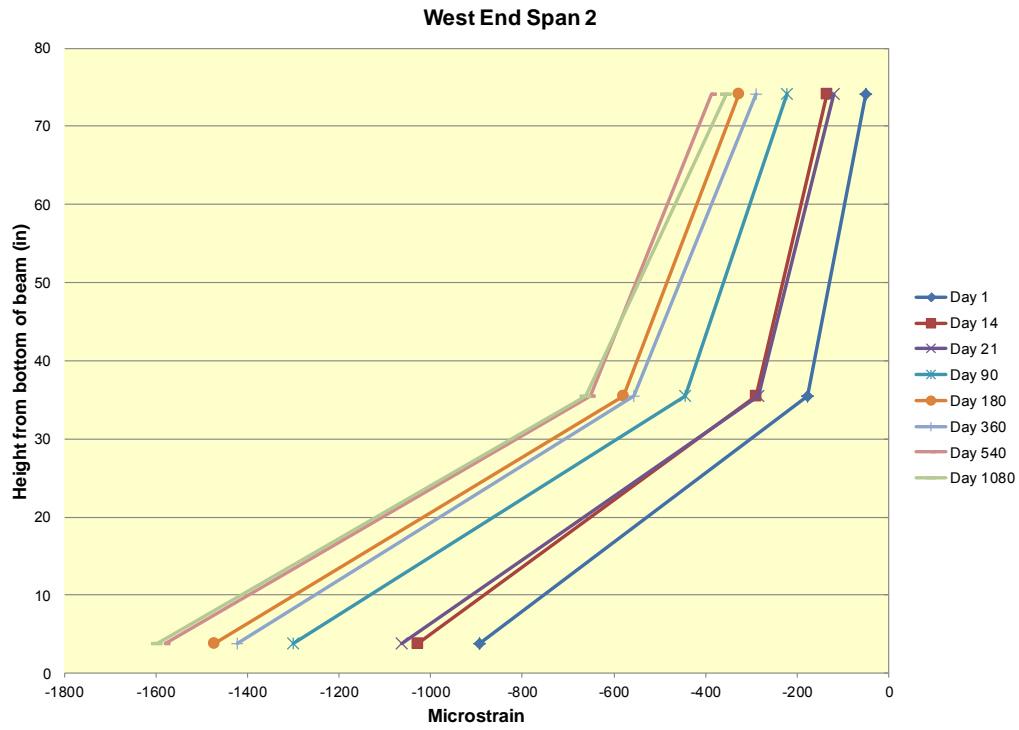


FIGURE C.7
Strain along Height of West End of Span 2

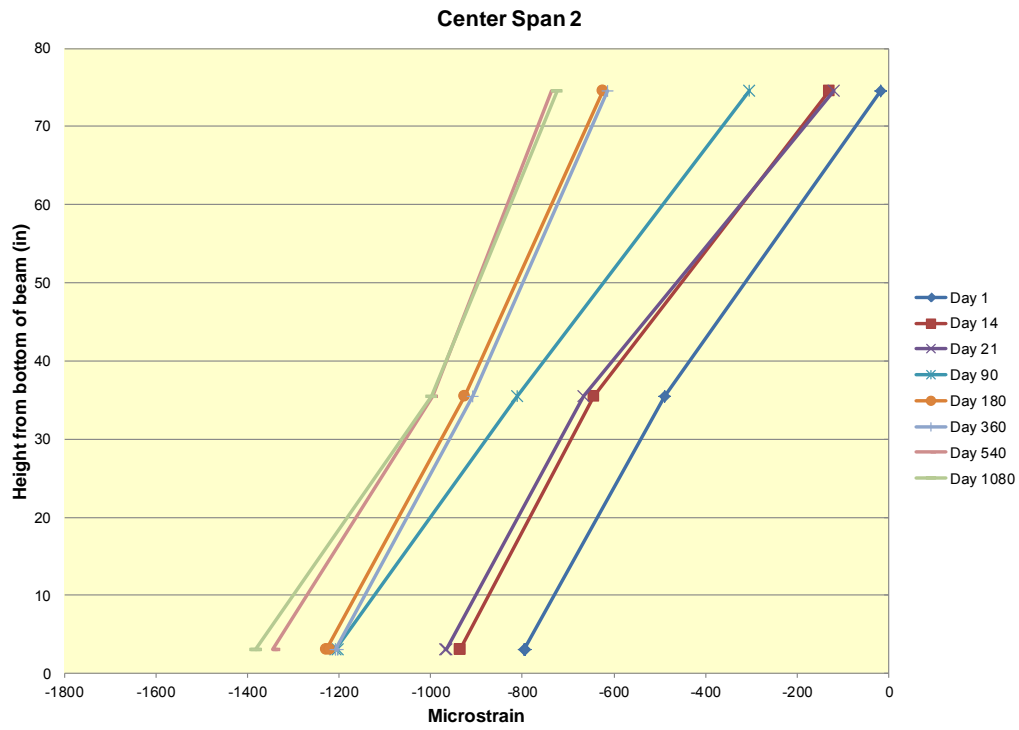


FIGURE C.8
Strain along Height of Center of Span 2

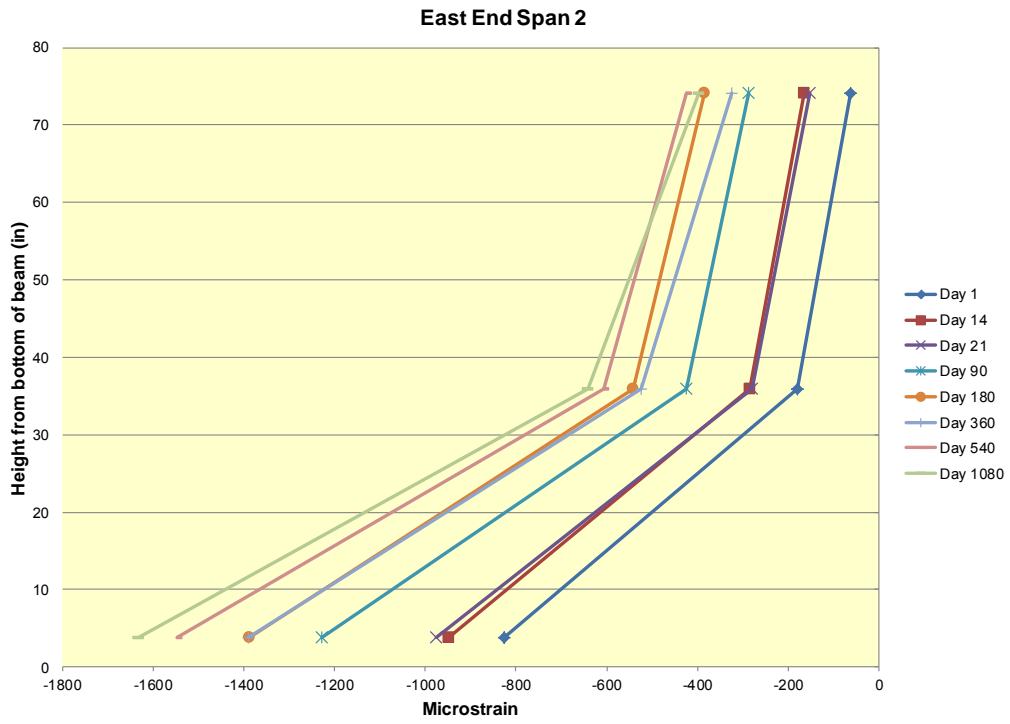


FIGURE C.9
Strain along Height of East End of Span 2

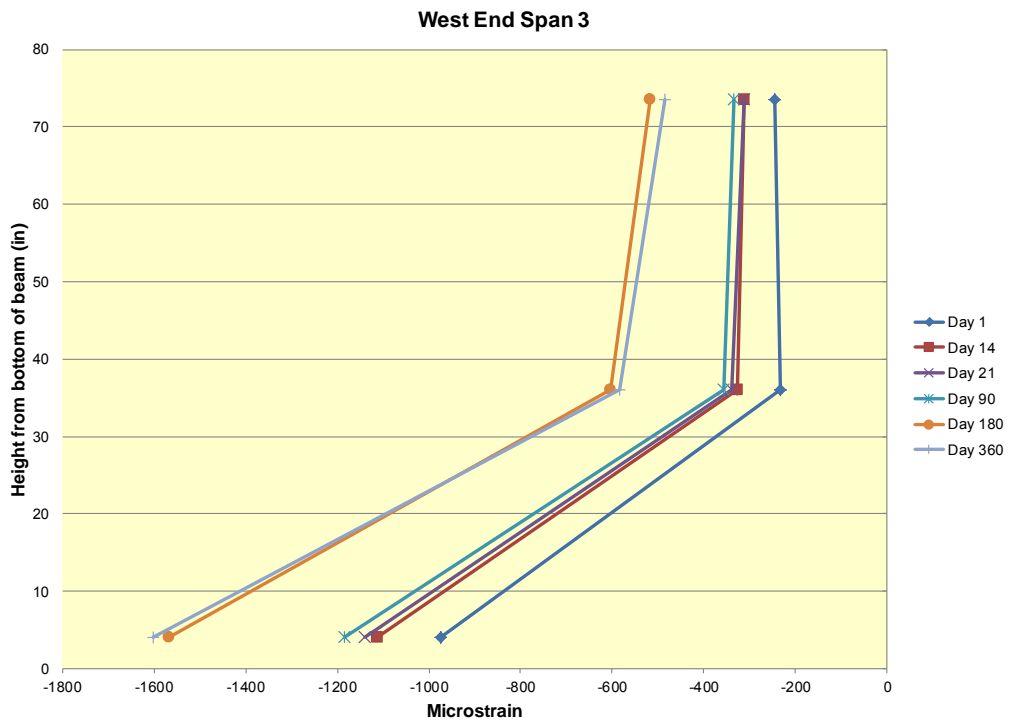


FIGURE C.10
Strain along Height of West End of Span 3

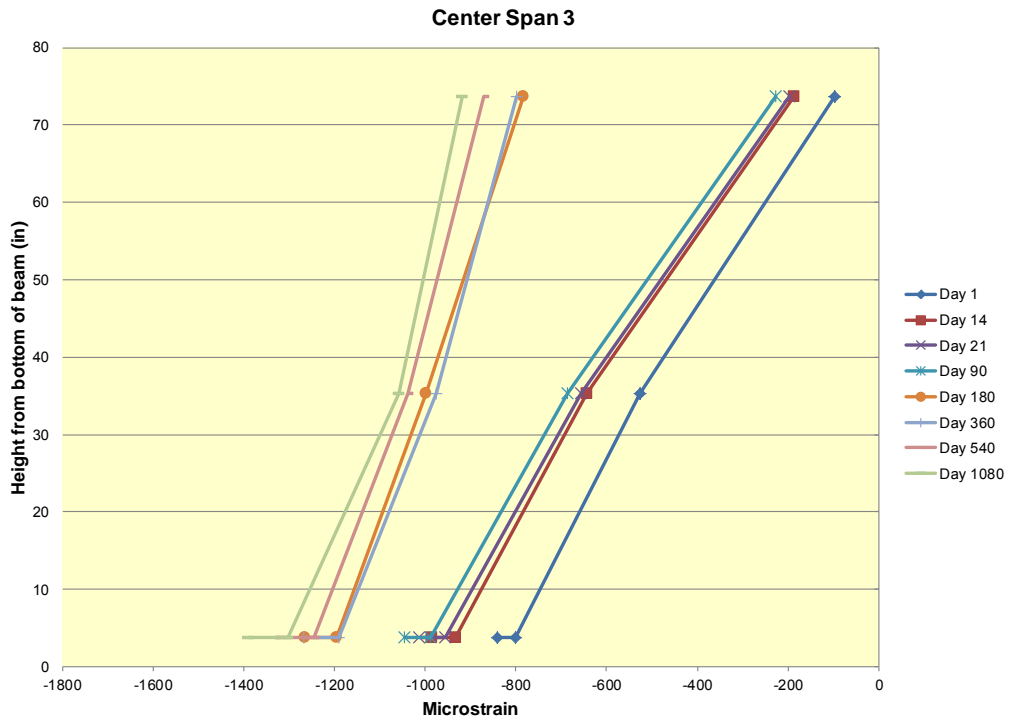


FIGURE C.11
Strain along Height of Center of Span 3

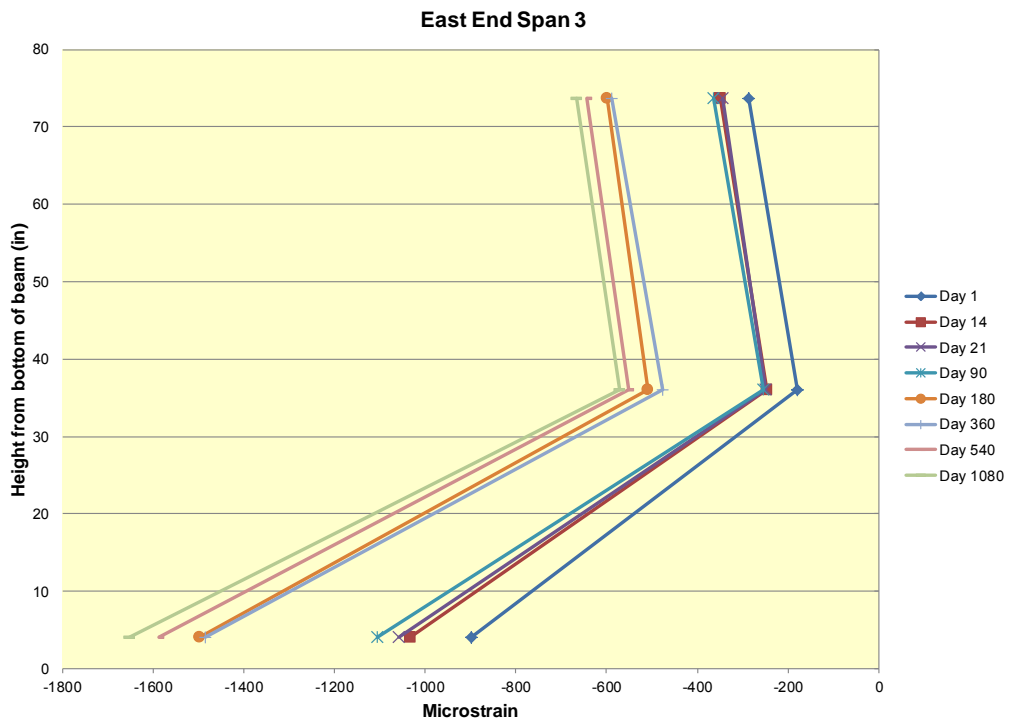


FIGURE C.12
Strain along Height of East End of Span 3

K-TRAN

KANSAS TRANSPORTATION RESEARCH AND NEW-DEVELOPMENT PROGRAM

